This is a preprint, the final version is subject to change, of the American Mineralogist (MSA)
Cite as Authors (Year) Title. American Mineralogist, in press.
(DOI will not work until issue is live.) DOI: http://dx.doi.org/10.2138/am-2016-5427

Trace Element Thermometry of Garnet-Clinopyroxene Pairs
Revision 1

Jonathan R Pickles[1,2], Jonathan D Blundy[2] and Richard A Brooker[2]

[1]Camborne School of Mines, University of Exeter, Penryn Campus, Penryn, TR10 9FE. UK
[2]School of Earth Sciences, University of Bristol, Wills Memorial Building, Bristol BS8 1RJ, UK

Abstract

We present major and trace element data on coexisting garnet and clinopyroxene for experiments carried out between 1.3 and 10 GPa and 970 and 1400 °C. We demonstrate that the lattice strain model, which was developed for applications to mineral-melt partitioning data, can be adapted to garnet-clinopyroxene partitioning. Using new and published experimental data we develop a geothermometer for coexisting garnet and clinopyroxene using the concentration of rare earth elements (REE). The thermometer, which is based on an extension of the lattice strain model, exploits the tendency of minerals at elevated temperatures to be less discriminating against cations that are too large or too small for lattice sites. The extent of discrimination against misfit cations is also related to the apparent elasticity of the lattice site on which substitution occurs, in this case the greater stiffness of the dodecahedral X-site in garnet compared with the 8-fold M2-site in clinopyroxene. We demonstrate that the ratio of REE in clinopyroxene to that in coexisting garnet is particularly sensitive to temperature. We present a method by which knowledge of the major and REE chemistry of garnet and clinopyroxene can be used to solve for the equilibrium temperature. This method is applicable to any scenario in which the two minerals are in equilibrium, both above and below the solidus, and where the mole fraction of grossular in garnet

is less than 0.4. Our method, which can be widely applied to both peridotitic and eclogitic paragenesis with particular potential for diamond exploration studies, has the advantage over commonly used Fe-Mg exchange thermometers in having a higher closure temperature because of slow interdiffusion of REE. The uncertainty in the calculated temperatures, based on the experimental data set, is less than ±80 °C.

Keywords: Lattice Strain Model, geothermometer, garnet, clinopyroxene, eclogite, experimental petrology, REE

Introduction

Deciphering the pressure (*P*) and temperature (*T*) conditions of deep earth processes using samples that are now exhumed to the surface requires a detailed understanding of the high-pressure phases and their chemistry over a range of relevant conditions. Such information has played an important role in the unraveling of *P*-*T* conditions during metamorphism and tectonic events. One industrial application involves diamond exploration where a particular challenge is establishing whether mantle-derived samples formed at *P* and *T* conditions conducive to diamond stability. In this context, the paragenesis of garnet (grt) + clinopyroxene (cpx) in rocks of mafic or ultramafic composition has focused attention on this mineral pair as potential geothermometers and barometers. A number of models exist to estimate equilibrium

52 temperatures of coexisting garnet and clinopyroxene (Raheim and Green 1974; Ellis and
53 Green 1979; Powell 1985; Ai 1994; Nakamura 2009; Sun and Liang 2015). The majority of these
54 thermometers rely on the Fe-Mg exchange between the garnet and clinopyroxene. For
55 example, the geothermometer of Ellis and Green (1979) utilizes the Fe-Mg exchange K_D
56 ($K_D = \frac{(Fe^{2+}/Mg)^{gnt}}{(Fe^{2+}/Mg)^{cpx}}$) between garnet and clinopyroxene. This method is widely used but
57 is susceptible to stoichiometrically-derived estimates of Fe^{3+} in the minerals that can
58 arise from cumulative errors in electron microprobe analyses (EMPA). This has been
59 clearly demonstrated by Li et al. (2005) who measured the Fe^{2+}:Fe^{3+} ratio with Mössbauer
60 and compared this to the ratio calculated by stoichiometry using EMPA. Li et al. (2005)
61 found that in every instance the ratios were different. However it should be noted that
62 advances are being made to EMPA methodology (Matjuschkin et al. 2014) and increasingly
63 XANES is being used to estimate garnet Fe^{2+}:Fe^{3+} ratios (Berry et al. 2010; Hanger et
64 al. 2015). Although there are alternative permutations to the thermometer of Ellis and
65 Green (1979) most methods rely on the Fe-Mg K_D. A further limitation with this type
66 of thermometer can arise through the relative ease of resetting of this exchange
67 during cooling. For these reasons exchange of slow-diffusing trace elements
68 between garnet and clinopyroxene has potential as a more reliable alternative
69 geothermometer, e.g. (Sun and Liang 2012, 2013, 2015). The trace element
70 concentrations of garnet and clinopyroxene from eclogite and garnet peridotite are
71 routinely measured (for example Harte and Kirkley (1997); Appleyard et al. (2007); Gréau
72 et al. (2011)), often as an aspect of diamond exploration strategies. However,
73 interpreting the trace element data is less routine (Griffin and Ryan 1995). Here we further

74 explore the use of trace element contents of coexisting garnet and clinopyroxene as a
75 geothermometer.

76 Early work by Goldschmidt (1937) demonstrated that trace elements enter
77 specific mineral sites and he proposed that ionic charge and radius strongly influence
78 trace element uptake, as measured, for example, by the partition coefficient for a trace
79 element between coexisting phases. Based on the thermodynamic work of Nagasawa
80 (1966) and Brice (1975), Blundy and Wood (1994) and Wood and Blundy (1997)
81 developed the lattice strain model which allows for the prediction of trace element
82 partitioning between a mineral and melt as a function of temperature, pressure and
83 mineral composition (X). The model describes how readily an element, i, with a
84 known ionic radius, r_i, will be incorporated into a crystal lattice. Blundy and Wood
85 (1994) and Wood and Blundy (1997) describe the incorporation of trace ions into
86 crystal lattices via the lattice strain model:

87

88 **(2003)** $$D_i = D_o \exp\left(\frac{-4\pi E N_A\left[\frac{r_o}{2}(r_i - r_o)^2 + \frac{1}{3}(r_i - r_o)^3\right]}{RT}\right)$$

89 **Equation 1**

90

91 Where D_i is the partition coefficient of element i between crystal and melt, D_o is
92 the theoretical strain-free partition coefficient, E is the apparent Young's modulus of
93 the lattice site, N_A is Avogadro's Number and r_o is the ideal cation size for the lattice
94 site of interest. Based on this model Wood and Blundy (1997) give equations to

95 predict each term for clinopyroxene-melt partitioning of rare earth elements (REE),
96 and van Westrenen et al. (1997) and van Westrenen and Draper (1999) give
97 equivalent terms for garnet-melt partitioning of REE.

98 Figure 1, a schematic representation of the lattice strain model, shows that
99 as the cation radius, r_i, deviates from r_o so the partition coefficient decreases. A
100 large Young's Modulus, E, will narrow the parabola making it harder for the lattice to
101 accommodate a misfit ion. Wood and Blundy (1997) showed that the parabola is
102 lattice site- and cation charge-dependent. The latter dependency arises because
103 heterovalent substitutions in minerals (e.g. Nd^{3+} for Ca^{2+}) require charge-balancing
104 coupled substitutions even when the mismatch between host and substituent ionic
105 radii is very small (Wood and Blundy 2001). In most rock-forming minerals a
106 wide range of charge-coupled substitutions is possible (e.g. $Nd^{3+} + Al^{3+} = Ca^{2+} + Si^{4+}$
107 or $Nd^{3+} + Na^{+} = 2Ca^{2+}$ in clinopyroxene; Wood and Blundy (1997)). The challenge is
108 to find the substitution mechanism that is most energetically favorable and best
109 suited to the bulk chemistry of the system.

110 Temperature and pressure also play a role in influencing the partition
111 coefficient. An increase in T and a decrease in P allow the crystal lattice sites to be
112 more flexible, i.e. reduce their effective E, which in turn allows them to accommodate
113 misfit cations more easily. Note also that T appears in the denominator to Equation 1
114 so that at very high temperatures all mineral-melt partition coefficients approach
115 unity.

116 The success of the lattice strain model for mineral-melt pairs, lies primarily
117 in the fact that the shear moduli of silicate melts are zero, hence $E^{melt}=0$.

Consequently from a purely lattice strain point of view there is no mechanical energy associated with replacing one ion with another in a silicate melt. In reality this is unlikely to be true, especially as other factors influence trace element incorporation into melts, such as co-ordination environment, complexation, configurational entropy etc. Experimental studies of melt-melt partitioning (e.g. Watson (1976), Ryerson and Hess (1978), Schmidt et al. (2006)) reveal that elements in general partition unequally between melts of different composition reflecting the energetic preferences of ions with different charges and/or radii for melts with different compositions/structures. However, the magnitude of melt-melt partition coefficients is always smaller, by several orders of magnitude, than that of mineral-melt partition coefficients for the same range of ionic radii and charge, demonstrating that it is the energetics of trace ion incorporation into minerals that dominates the energetics of mineral-melt exchange equilibria. Moreover, atomistic simulations in which ions are substituted onto lattice sites and the resultant relaxation (strain) energies calculated (e.g. Allan et al. (2003)) corroborate the findings of mineral-melt partitioning studies.

Having established that it is the energetics of trace ion incorporation into crystals that dominates mineral-melt partitioning equilibria it is a simple matter to show that an understanding of mineral-melt partitioning for Mineral 1 and for Mineral 2 constitutes an approach to understanding trace element partitioning between Mineral 1 and Mineral 2. The object of this paper is to explore the possibility of extending the lattice strain models for clinopyroxene-melt and garnet-melt towards a better understanding of garnet-clinopyroxene partitioning. Through experiments we

investigate the mineral-mineral partitioning of elements, rather than mineral-melt. Lee et al. (2007) used this approach to develop a version of the lattice strain model that describes trace element partitioning between olivine and cpx, which we have modified here for the case of partitioning between garnet and cpx. As our reference element we have chosen Y instead of Lu, which was used by Lee et al. (2007), due to the greater availability of reliable Y data (Y has a natural abundance approximately 60 times greater the Lu).

$$D_i^{grt/cpx} = D_Y^{grt/cpx} . \exp\left(\frac{-4\pi N_A}{RT} \left[\frac{1}{2}\left(r_Y^2 - r_i^2\right)\left(E_{grt} r_o^{grt} - E_{cpx} r_o^{cpx}\right) + \frac{1}{3}\left(r_i^3 - r_Y^3\right)\left(E_{grt} - E_{cpx}\right) \right] \right)$$

Equation 2

By referencing the model to an element it obviates the need to explicitly evaluate the ratio of D_o parameters for garnet and cpx that appear in the mineral-melt formulations of the lattice strain model (Equation 1). Moreover, as all of the parameters in the exponential on the right hand side of Equation 2 can be calculated for the P-T-X of interest using existing models for cpx-melt and garnet-melt partitioning, so D_Y is a fit parameter for the experimental data. To add to this current methods of calculating D_o require knowledge of the melt composition and as D_o is not a true equilibrium constant we feel that this is a robust approach.

To test our model we performed a series of experiments aimed at investigating the partitioning of trace elements, particularly the rare earth elements (REE) and Y, between garnet and clinopyroxene, using a flux, e.g. a silicate melt, to promote crystal growth. The new experimental dataset is augmented by published experimental data on garnet-clinopyroxene pairs. Conditions of the new experiments

were designed so as to increase the coverage of P -T –X space. We will use our experimental dataset to (a) investigate extension of the Lee et al. (2007) approach to garnet and clinopyroxene (b) critically appraise the recent mineral-mineral partitioning work by Sun and Liang (2015, 2013, 2012) and (c) develop a REE geothermometer for coexisting garnet and cpx. We use experimental garnet and cpx from both eclogitic and peridotitic bulk compositions to increase the applicability of the models. In all cases the Nernst partition coefficient, D_i, is defined as the weight concentration of the element i in garnet divided by the concentration of i in cpx. Thus D_i is shorthand for $D^{grt/cpx}$.

Methods

Experimental Methods

Experimental starting materials (supplementary data table S1) consisted of either a mechanical mixture of synthetic oxides (SiO_2, TiO_2, Al_2O_3, Fe_2O_3, MnO, MgO) and carbonates ($CaCO_3$, Na_2CO_3, K_2CO_3) or a natural basanitic glass. Starting materials were doped with trace elements chosen to represent the different geochemical groups (HFSE, REE, LILE etc.) but also in a way that minimizes analytical interferences during analysis. Analytical grade oxides of SiO_2, MgO and Al_2O_3 were dried at 1000 °C for 2 hours. Other oxides and carbonates were oven dried at 200 °C for 24 hours. All oxides and carbonates were then stored either in a desiccator or an oven at 110 °C prior to mixing. Reagents were mixed in appropriate proportions and ground under acetone to homogenize and reduce the grain size. The mixture was decarbonated at 600 to 1000 °C over a minimum of 12 hours.

186 Starting material JP 1 (Table S1) is based on analyses of an eclogite xenolith
187 from the Roberts Victor mine. A synthetic hydrous "rhyolite" flux, based on a partial
188 melt in equilibrium with an eclogitic residue at subduction zone conditions (Klimm et
189 al. 2008), was mixed with the synthetic garnet powder and synthetic cpx powder to
190 enhance the equilibration rates on the timescales of experiments. The use of a
191 fluxing agent has previously proven to be successful in the case of zircon-garnet
192 partitioning by Rubatto and Hermann (2007). The rhyolite flux was formulated
193 using dried oxides and carbonates, as above, but alkalis were added as natural albite
194 and K-feldspar. For experimental run temperatures below 1300 °C 10 wt.% deionized
195 water was added with a micro-syringe. Finally, the flux, the synthetic garnet and cpx
196 powders were mixed in the desired proportions and ground under acetone to
197 further homogenize. The weight proportions used for JP1 were 20:40:40,
198 flux:garnet:cpx. Of the other starting materials, ZrTi is a 25:25:50 mixture of
199 synthetic oxide mixes of grossular, pyrope and diopside, with extra Zr and Ti to
200 saturate with zircon and rutile, BAS is a natural basanitic glass used in experiments
201 by Green et al. (2000), AOB is a synthetic alkali olivine basalt based on previous
202 work by Withers (1997) and NSR-16 is a synthetic basaltic glass, similar in
203 composition to a 12.8 Ma transitional low-K basalt, from the Little North Santiam
204 River area of Oregon in the Western Cascades volcanic arc (R.M. Conrey, written
205 comm). Crystal seeds were not used in any experiments. These different starting
206 materials were chosen to generate garnet and cpx across a wide variation in bulk
207 composition.

208 Trace elements were added to all starting materials as ICP-standard nitrate

209 solutions using a micropipette and dried under a heat lamp. The doped mixtures
210 were re-homogenized in an agate mortar and denitrified at 300 °C. As the BAS glass
211 is natural and already contains a wide range of trace elements only 200 ppm of Li
212 were added. JP 1, ZrTi, AOB and NSR-16 had a complete suite of trace elements added.
213 The trace element contents of all starting materials are given in Table S2. Following
214 doping and denitrification starting materials JP 1, ZrTi and AOB were melted and
215 quenched in a controlled atmosphere, vertical quench furnace at an fO_2 equivalent
216 to the nickel-bunsenite (NNO) buffer, between 1000 and 1520 °C. This fixes the
217 Fe^{2+}:Fe^{3+} ratio in the starting material to match the intrinsic fO_2 of the experimental
218 apparatus and thereby minimizes redox reactions, mediated by H_2 diffusion, taking
219 place during the experiments. The exact 'intrinsic' fO_2 of the various apparatus is
220 unknown but anecdotal evidence suggests it is above NNO. NSR-16 was prepared as
221 a hydrous glass, using $Al(OH)_3$ as a source of H_2O. This trace element-doped powder
222 was loaded into an Au80:Pd20 capsule and held at 0.22 GPa and 1000 °C for 2 hrs in a
223 rapid-quench TZM cold-seal apparatus at NNO+1. To minimize Fe loss during
224 experiments the capsule material was a gold palladium alloy (Au80:Pd20). All
225 capsules were annealed and acid-cleaned before loading and welding. The outside
226 diameter of the capsules was 2 mm and they ranged in length from 0.5 to 2 mm. Some
227 experiments were run with two capsules each containing different starting
228 materials in end-to-end configuration.

229 Experiments from 3.0 to 3.4 GPa pressure were carried out using 1/2" end-
230 loaded piston cylinder apparatus at the University of Bristol. The pressure media

were NaCl, Pyrex and crushable alumina with a graphite furnace. The experiments were pressurized and heated simultaneously with the pressure always being the final variable to be increased, i.e. hot piston-in technique. During the experiment the pressure was manually maintained at the desired value and the temperature was measured using an axial $W_{95}Re_5$-$W_{75}Re_{25}$ thermocouple (not corrected for pressure) and regulated by a Eurotherm controller. The pressure correction of McDade et al. (2002b) was applied and verified by bracketing the quartz-coesite boundary. RB627 (1.3 GPa) was performed in a 3/4" talc/Pyrex assembly with a tapered graphite furnace and pressure-calibrated using the melting point of CsCI (see McDade et al. (2002a)).

Experiments at pressures greater than 3.4 GPa were carried out using a Walker-type multi-anvil apparatus at Bayerisches Geoinstitut (B.G.I.), University College London (U.C.L.) and the University of Bristol. In each case the pressure medium was precast MgO octahedra with truncations of varying length depending on the pressure required. Either an MgO or alumina spacer surrounded the capsule with a ZrO_2 insulator around the furnace. Experiments at B.G.I. used the 10/4 assembly with a $LaCrO_3$ furnace, at U.C.L. a 14/8 assembly with a graphite furnace and at Bristol an 18/11 assembly with graphite furnace. The temperature was measured with a $W_{97}Re_3$-$W_{75}Re_{25}$ thermocouple, inserted radially in U.C.L. experiments and axially at B.G.I. and Bristol. The experiments were pressurized over 3 hours and heated for between 6 and 8 hours. The pressure calibrations used the following phase changes: quartz-coesite, coesite-stishovite, Bi I-II, Bi III-V and $CaGeO_4$ (garnet to pervoskite). All experiments were ended by turning the power off to give quench times of less

254 than 10 seconds to reach 300 °C.

255 **Analytical Methods**

256 Major element data were collected using the Cameca SX100 electron
257 microprobe at the University of Bristol. For both garnet and cpx the beam
258 conditions were 20 kV, 20 nA beam and 1 μm spot size. Peak count times ranged
259 from 10 to 30 s depending on the concentration of the element of interest.

260 The Cameca IMS-4f ion-microprobe at the University of Edinburgh was used to
261 measure trace elements in garnet and cpx of the experimental run products by
262 secondary ion mass spectrometry (SIMS). All samples had a 20 nm gold coat applied
263 under vacuum. A primary beam of $^{16}O^-$ with a net impact of energy of 15 keV was
264 used. Positive secondary ions were accelerated to 4500 V with an energy offset of 75
265 eV and a window of 40 eV to minimize transmission of molecular ions. The beam
266 current was varied as necessary to permit analysis of the smaller grains because, in
267 general, beam diameter is a strong function of beam current, i.e. 30 μm beam
268 diameter at 5 nA, 15 μm at 1.5 nA. All SIMS pits were examined subsequently by
269 SEM to check that there was no visible overlap onto adjacent phases. Secondary ion
270 yields were calibrated using standard glass NIST SRM 610 (Hinton 1990) and
271 checked using secondary standards of garnets DD1 (Irving and Frey 1978), AP, SG
272 and cpx SC8804 (van Westrenen 2000). The following positive secondary ion masses
273 were analyzed and ratioed to ^{30}Si (as determined by electron microprobe): ^{7}Li, ^{11}B,
274 ^{30}Si, ^{42}Ca, ^{44}Ca, ^{45}Sc, ^{47}Ti, ^{51}V, ^{59}Co, ^{69}Ga, ^{88}Sr, ^{89}Y, ^{90}Zr, ^{93}Nb, ^{138}Ba, ^{139}La, ^{140}Ce, ^{143}Nd,
275 ^{149}Sm, ^{151}Eu, ^{157}Gd, ^{159}Tb, ^{267}Er, ^{171}Yb ^{175}Lu, ^{178}Hf, ^{181}Ta, ^{208}Pb, ^{232}Th, ^{238}U. (Note that

276 ^{71}Ga was used for the NIST610 glass due to overlap on ^{69}Ga of ^{138}Ba, a species with
277 negligible concentration in garnet and clinopyroxene.) The count times per cycle
278 were 5 s for all isotopes, except: 2 s for Si and ^{42}Ca, 3 s for ^{140}Ce, ^{47}Ti and ^{88}Sr, 7 s for
279 ^{143}Nd and ^{149}Sm and 10 s for ^{178}Hf. The number of cycles was between 8 and 15 to
280 produce statistically significant data, with low counting error. Isobaric oxide
281 interferences were greatly minimized by the careful choice of elements, doping levels
282 and energy filtering of secondary ions. The remaining molecular interferences, such
283 as ^{29}Si^{16}O on ^{45}Sc, were removed by conventional peak- stripping. Overlap of LREE
284 oxides on HREE was corrected using in-house REEO/REE values for cpx and values of
285 van Westrenen (2000) for garnet. Analysis of secondary standards demonstrated that
286 there was no significant secondary ion-yield differences between garnet and cpx thus
287 D_i is taken to be the Si-normalized concentration of an element in garnet divided by
288 that in cpx.

289 **Results and Discussion**
290
291 Experimental run conditions and major element mineral data measured by EMPA are
292 presented in Table 1 and Table 2. Experimental runs times were between 4 and 123
293 hours, see Table 1. We note that for the basanite runs these run durations are identical to
294 those of Green et al (2000) for the same starting materials and run conditions. Attainment
295 of equilibrium in the new experiments is demonstrated through the homogeneity of the
296 SEM images (Figure 2) combined with the small standard deviation in the major element
297 data, Table 1 and Table 2, along with the shape of the parabolae of the REE data.
298 The presented EMPA data for each experiment is a mixture of core and rim measurements,
299 therefore any variability within a crystal, i.e. zoning, would result in a large standard

deviation in the major element data. A total of 12 experiments contained garnet and cpx crystals between 20 and 100 μm that could be analysed by ion-microprobe. Occasionally garnets contained cpx inclusions, which were avoided during analysis. Areas of melt or quench crystals occurred in some experiments. The garnet and cpx end members were calculated using the methods of Deer et al. (1992) and Morimoto et al. (1988) respectively. SIMS trace element data for cpx are presented in Table 3 and for garnet in Table 4. Care was taken during data processing to check that there was no contamination by other phases during analysis. One clear indication of glass contamination is elevated concentrations of highly incompatible elements, such as U or Th. In some cases contamination only involved a few analytical cycles and these were eliminated during processing. In cases where there was persistent contamination throughout the analysis the trace element data were discarded.

The major element composition of garnet varies very little between each bulk composition. All garnets are pyrope-rich (0.65-0.41 mol fraction) with lesser amounts of grossular (0.26-0.14 mol fraction) and almandine (0.32-0.07 mol fraction), where almandine was calculated from stoichiometric Fe^{2+}. The only experiment with a greater almandine than grossular content is RB627. The majority of the experimental cpx are Na-rich (omphacite following the classification of Morimoto et al. (1988)) with three being relatively Mg-rich and falling within the Ca-Fe-Mg quadrilateral. Al^{iv} ranges between 0.175-0.003 cations per formula unit (c.p.f.u.), Na 0.507-0.108 c.p.f.u., Ca 0.757-0.475 c.p.f.u., Mg 1.049-0.539 c.p.f.u. and Fe 0.375-0.069 c.p.f.u. The concentration of Ca in both garnet and cpx increases with an increase in pressure, however the rate of change per GPa is greatest in garnet, which may have potential

323 as a barometer, although this is not explored here.

324 The high Fe^{3+} content of the garnets and most cpx (Table 1 and Table 2) is
325 consistent with the assumption of a run fO_2 above NNO. For instance, the average
326 calculated garnet Fe^{3+}/Fe^{tot} is 26% (range 8-41%; See Table 2) which is closer to the
327 $ReReO_2$ buffered runs (~NNO+2) of Matjuschkin et al. (2014) than the 5% Fe^{3+}/Fe^{tot} in
328 garnets of the NNO runs of Rubatto & Hermann (2007). Note that at these high fO_2
329 values it is anticipated that >90% of the Eu can be considered as trivalent (see Burnham
330 et al. (2015)).

331 Garnet-cpx trace element partition coefficient data, Figure 3, show that the
332 differing bulk compositions produce similar trends. In all experiments Sr has the
333 smallest garnet-cpx partition coefficient. The absolute concentration of Sr increases
334 greatly in both garnet and cpx with an increase in pressure, however the change in
335 concentration is similar in both minerals resulting in a modest increase in D_{Sr} with
336 *P*. A comparable effect is seen in Li with *P* except that the concentration in garnet
337 increases more quickly than cpx resulting in a potential barometer. This effect has
338 been previously identified by Hanrahan et al. (2009, 2009b). Lutetium has the
339 highest partition coefficient in all experiments.

340

341 **Lattice Strain Model Applied to Garnet-Cpx Pairs**

342 Our new data on REE partitioning between the dodecahedral X-site in garnet and
343 the 8-fold M2 site in cpx are in agreement with previous studies. Figure 4 and Figure
344 5 show the partition coefficient plotted against the ionic radius of the cation in 8-
345 fold coordination, using ionic radii values from Shannon (1976). There is an

346 increase in concentration from La to Lu in both minerals, however the LREE have a
347 greater affinity for cpx than garnet, whereas HREE more readily enter garnet. The
348 change in the REE concentration in garnet, from LREE to HREE, is far greater than
349 that of cpx. The concentration of Sm is approximately equal in garnet and cpx,
350 resulting in a partition coefficient of around 1. Garnet-melt and cpx-melt data have
351 been shown to form parabolae by van Westrenen (2000) and Wood and Blundy
352 (1997) respectively. By combining the two mineral-melt parabolae, as we
353 effectively do here, we see an almost linear trend. This is in part because Sc is not
354 considered here as it enters the cpx M1 site rather than the M2 site which
355 accommodates the REE (Allan et al. 2003). Consequently, we only observe one limb
356 of what is still a parabola. One of the objectives of this paper is to investigate the
357 ability of the lattice strain model to describe partitioning between garnet and cpx.
358 To this end we have used the equations of Wood and Blundy (1997) and van
359 Westrenen and Draper (2007) to derive the lattice strain parameters r_o^{cpx}, E^{cpx}, r_o^{grt},
360 E^{grt}. We find that these parameters describe the data well. Figure 4 and Figure 5
361 show the curve of weighted best fit for the lattice strain model for the new
362 experimental data (Equation 2) having adopted the Wood and Blundy (1997) and
363 van Westrenen and Draper (2007) r_o and E terms for cpx and garnet respectively.
364 As all variables are known, i.e. *T, P* and composition, this demonstrates the
365 agreement between theory and the experimental data and confers a self-consistency
366 between the published mineral-melt and the new mineral-mineral models.

367 To further investigate the lattice strain approach, garnet-cpx partitioning data
368 from other experimental studies were also considered (Table S3). These

experiments cover a wide range of $P - T$ conditions (1000 to 1750 ^{o}C and 1.5 to 7.0 GPa). As with our experiments, the weighted curve of best fit to the garnet-cpx REE partition coefficients is calculated using Equation 2 with r_o and E for cpx and garnet calculated from Wood and Blundy (1997) and van Westrenen and Draper (2007) respectively. Most data are well described by the lattice strain model and the imposed lattice strain parameters (see Figure S1, Figure S2 and Figure S3). Poor agreement between the model and the data can often be attributed to the quality of the analyses. The experiments by Hauri et al. (1994) and Klein et al. (2000), for example, show many inconsistencies with the other datasets, possibly due to contamination by glass or cpx in the garnet analyses. For this reason these data were not included in further analysis. The experiments by Kuzyura et al. (2010), however, have small analytical uncertainties and no obviously anomalous results, yet the model provides a poor fit to the data (Figure S2). The primary difference between these experiments and all the others is that Kuzyura et al. (2010) used a carbonate-silicate mix, as opposed to silicate only. This results in garnets with a much greater Ca content (around 0.5 mole fraction grossular end-member as opposed to between 0.1 and 0.2 in the other experiments). The effect of Ca on REE partitioning was investigated by van Westrenen et al. (1999) who found that as the grossular component in garnet increases E^{grt} decreases. van Westrenen and Draper (2007) provide a correction for Ca in the r_o^{grt} term which is then used to calculate E^{grt}. In many instances this is acceptable however in very Ca-rich garnets this approach breaks down, as shown by the Kuzyura et al. (2010) experiments. As the experiments by Kuzyura et al. (2010) are extreme in their Ca content they are not

included in the temperature comparisons in this study. We do suggest that further work is required to fully quantify the effect of high-Ca on E^{grt}.

Sun and Liang (2012, 2013) present a model for garnet-cpx partitioning of REE in which they define new terms for predicting E and r for both minerals. A comparison of the r_o^{cpx} and E^{cpx} values obtained by Sun and Liang (2012) to those of Wood and Blundy (1997) shows very good agreement. However, for r_o^{grt} the term of Sun and Liang (2013) is calculated using only the Ca content of garnet and E^{grt} is only dependent on r_o^{grt}. The result is that both parameters in garnet are defined solely by the Ca content. Previous work by van Westrenen et al. (1999); van Westrenen (2000); van Westrenen and Draper (2007) demonstrated that E^{grt} is heavily dependent on a number of other garnet compositional terms, in addition to *T* and *P*. Comparing the E^{grt} values calculated through the method of Sun and Liang (2013) with those calculated with the method of van Westrenen and Draper (2007) demonstrates little correlation between the values (Figure 6). The method of Sun and Liang (2013) underestimates the majority of the E^{grt} by several hundred GPa compared to the method of van Westrenen and Draper (2007). E^{grt} values from the two experiments by Kuzyura et al. (2010) are overestimated by around 250 GPa.

Calculating E^{cpx}, r_o^{cpx}, E^{grt} and r_o^{grt} using the method of Sun and Liang (2013, 2015) and comparing the fit to the experimental data, analogous to figures Figure 4 and Figure 5, demonstrates little correlation between the fit and the data. The mismatch can be attributed entirely to the value of E^{grt}. Figure 6 indicates that using only Ca in garnet to calculate both E^{grt} and r_o^{grt} is not robust. Whilst the method given by Sun and Liang (2013) aids in predicting temperature and pressure their

E^{grt} values are inconsistent with garnet-melt experimental data.

Lattice Strain Model and Temperature

The partitioning of trace elements between garnet and cpx given by Equation 2 has an inherent T term. Based solely on Equation 2, a change in the partitioning with T is predicted, both through its occurrence in the denominator of the exponential terms and in its tendency to reduce E and increase r_o. In contrast, although pressure will also affect E and r_o the magnitude of this effect is relatively small, compared to that of temperature. The influence of temperature was confirmed by the work of Wood and Blundy (1997) and van Westrenen and Draper (2007) who found that E in both cpx and garnet has a quantifiable temperature dependence. Dohmen and Blundy (2014) came to a similar conclusion from a study of plagioclase-melt trace element partitioning. Figure 7 confirms the importance of T by displaying the change in the shape of the parabola when all the terms are kept constant and only T is altered. Equation 2 can be re-arranged to make T the dependent variable and therefore give a geothermometer that can be applied to REE partitioning between coexisting garnet and cpx.

$$D_i^{grt/cpx} = D_j^{grt/cpx}.\exp\left(\frac{-4\pi N_A}{RT}\left[\frac{1}{2}\left(r_j^2 - r_i^2\right)\left(E_{grt}r_o^{grt} - E_{cpx}r_o^{cpx}\right) + \frac{1}{3}\left(r_i^3 - r_j^3\right)\left(E_{grt} - E_{cpx}\right)\right]\right)$$

This is a preprint, the final version is subject to change, of the American Mineralogist (MSA)
Cite as Authors (Year) Title. American Mineralogist, in press.
(DOI will not work until issue is live.) DOI: http://dx.doi.org/10.2138/am-2016-5427

$$T(K)=\frac{\frac{-4\pi N_A}{R}\left[\frac{1}{2}\left(r_j^2-r_i^2\right)\left(E_{grt}r_o^{grt}-E_{cpx}r_o^{cpx}\right)+\frac{1}{3}\left(r_i^3-r_j^3\right)\left(E_{grt}-E_{cpx}\right)\right]}{\ln\left(\frac{D_i}{D_j}\right)}$$

Equation 3

Where *j* is any REE other than *i.* As three of the parameters in the lattice strain model (E^{cpx}, E^{grt} and r_o^{grt}) require temperature to be known an iterative approach was adopted to solve for the temperature. This negates the need for developing new, temperature-independent methods for calculating each of these variables and consequently compliments the mineral-melt partitioning work of previous studies. We consider it essential that any garnet-cpx partitioning model is consistent with garnet- and cpx-melt partitioning, rather than invoking a set of new, best-fit lattice strain parameters for one or both minerals.

To calculate temperature we use the partition coefficients of two rare earth elements (replacing *i* and *j* in Equation 3), Equation 3 and the lattice strain parameters as defined by Wood and Blundy (1997) and van Westrenen and Draper (2007). For clarity, the lattice strain terms given by Wood and Blundy (1997) and van Westrenen and Draper (2007), where P is in GPa and T is absolute temperature in Kelvin, are:

$$E^{cpx}=318.6+6.9P-0.036T$$
$$r_o^{cpx}=0.974+0.067X_{Ca}^{M2}-0.051X_{Al}^{M1}$$
$$r_o^{grt}=0.9302X_{Py}+0.993X_{Gr}+0.916X_{Alm}+0.946X_{spes}+1.05\left(X_{And}+X_{Uv}\right)$$
$$-0.0044(P-3)+0.000058(T-1818)$$
$$E^{grt}=2826(1.38+r_o^{grt})^{-3}+12.4P-0.072T+237\left(Al+Cr\right)$$

451

452 Any two REE can be chosen to replace *i* and *j* in Equation 3 but it is preferable
453 to choose two elements that have a large relative difference in ionic radius and exist
454 in concentrations high enough to return accurate measurements. An important
455 consideration is the precision of the REE analysis. LREE are invariably in very low
456 concentration in natural garnet and subject to considerable analytical uncertainty. To
457 minimize the error in our temperature prediction we calculated the temperature
458 using multiple REE pairs and compared the weighted mean to the experimental
459 temperature. We assumed that calculating the temperature with multiple pairs
460 avoids too much weight being placed on one erroneous datum. The elements not used
461 in the temperature calculations are La and Ce as they are in very low concentration in
462 garnet and Tb, Dy and Ho as they are often not included in experimental charges.
463 For each temperature calculation the terms in the lattice strain model were
464 calculated with an initial best-guess temperature in order to derive the
465 temperature-dependent terms on the right hand side of Equation 3. The
466 temperature was then adjusted iteratively until the input and the calculated
467 temperature were the same to within 1 degree. The temperature for each element
468 pair, along with the error from the ion probe data, is used to calculate a weighted
469 mean for each experiment. This approach takes into account the uncertainty in the
470 trace element data. Calculated temperatures less than 600 or greater than 2000 ^{o}C
471 were assumed to be erroneous and removed from consideration. An excel
472 spreadsheet to perform these calculations is available from the first author.

Comparing the temperature calculated through our new method, which uses the lattice strain parameters of Wood and Blundy (1997) and van Westrenen and Draper (2007), with the experimental temperature shows very good agreement (Table 5 and Figure 8a). The mean absolute deviation between the temperatures, when the high-Ca experiments by Kuzyura et al. (2010) are disregarded, is only 76 °C. The broad range of bulk compositions for our validation experimental dataset demonstrate that our approach can be applied to any coexisting garnet-cpx pairs.

Applications

Although the majority of the garnet-cpx geothermometers in common usage utilize the major elements we believe that our rare earth element approach has a number of advantages.

1) The use of rare earth elements as a geothermometer has an advantage over the Fe-Mg exchange models as the slow diffusion of 3+ cations (van Orman et al. 2002) leads to a correspondingly higher closure temperature (Frost and Chacko 1989). Work by Pattison (1994) and others shows that the Fe-Mg exchange can return differing temperatures that depend on the grain size of the minerals analyzed. Pattison (1994) suggested that the Fe-Mg in granulites may record the temperature at which inter granular exchange ceased in the rock. By using REE, which diffuse much more slowly, the peak metamorphic temperature should be recovered. See Yao and Liang(2015) and Sun and Liang (2015) for detailed discussion of closure temperatures in bi-mineralic systems.

496 2) The REE geothermometer presented here is developed independently of
497 any other geothermometer. Other models, such as Witt-Eickschen and O'Neill
498 (2005), use natural xenoliths along with extant major element thermometers to
499 develop trace element geothermometers. Such models will therefore inherit any
500 inaccuracies from their "parent" model against which they are calibrated. This will
501 not be the case with our model as it has been developed independently of any pre-
502 existing geothermometer.
503 3) The thermometer developed here is entirely consistent with a
504 substantial body of garnet-melt and cpx-melt partitioning studies that have gone
505 some way to refining the key lattice strain parameters. We have not had to invoke
506 new lattice strain parameters for the specific purpose of recovering temperature
507 from garnet-cpx pairs.
508 4) Finally, the availability of a large number of REE data gives our
509 approach considerable flexibility in that different pairs of REE can be used,
510 according to data availability and precision. Through combining the temperature
511 predictions of multiple REE pairs the most accurate temperature can be estimated.
512 An enduring shortcoming of this and other thermometers is the need to
513 know the equilibrium pressure. Throughout this study where a pressure estimate
514 is required, such as in predicting E^{grt}, the experimental *P* has been used. Currently
515 the barometers of Simakov (2008) and Sun and Liang (2015) are available for
516 garnet-cpx pairs. Alternatively, many studies use an assumed pressure of 5 GPa to
517 compare data. To avoid including uncertainties inherent in the barometers and to
518 clearly display the error associated with our model we have only used experimental

519 pressures. An increase of 1 GPa in assumed pressure increases the temperature
520 estimate by, on average, 50 °C in our model irrespective of the REE pair chosen.

521 Our experiments show that the effect of pressure on rare earth element
522 partitioning in isothermal, isochemical experiments is not consistent enough to be used
523 as barometer. Comparing the isothermal experiments, Figure 9, for experiments
524 carried out at 1200 and 1400 °C shows that there is not a consistent effect of
525 pressure that can be used to solve for the pressure. The experiments carried out at
526 1200 °C, but variable pressure, are all within error of each other. The experiments
527 at 1400 °C appear to show a pressure effect, however, on closer inspection the effect
528 is not consistent.

529

530 **Comparison to existing thermometers**

531 The Fe-Mg exchange geothermometer of Ellis and Green (1979) is the most
532 widely used method of estimating temperature for garnet-clinopyroxene pairs. To
533 evaluate our new geothermometer we have calculated the temperature using the
534 method of Ellis and Green (1979), both with and without the calculation of Fe^{2+} by
535 stoichiometry. We have also calculated temperature for the same
536 experiments with the REE method of Sun and Liang (2015) and compared all
537 T estimates to the experimental temperature (Table 5). Points of note are that
538 temperature estimates for some of the experiments carried out during this study are
539 significantly over-estimated using the method of Ellis and Green (1979). Even when
540 the error associated with the Fe^{2+} calculation is removed ($T_{(EG^*)}$ in Table 5) the
541 temperature estimates are still several hundred degrees too high. This results in

a mean absolute deviation of 240 °C between the temperature calculated using the method of Ellis and Green (1979) and the experimental temperature. The mean absolute deviation between the experimental temperature and that calculated *T* using the method of Sun and Liang (2014) is 174 °C. This value is compared with our lattice strain approach which has an absolute mean deviation of only 76 °C when the temperature is calculated using the mean of all REE pairs. (The highly discrepant values for Kuzyura et al. (2010) data are not included in either of the REE models.) This clearly demonstrates that not only can the lattice strain model be used to estimate temperature but also the *T* is more accurate than the most commonly used eclogitic geothermometer. It should be reemphasized that our formulation is not calibrated on the experimental data presented in Table 5. We have simply transferred the lattice strain parameters from garnet-melt and cpx-melt models and applied them. Thus this is a fair test of all thermometers.

Implications

In this paper we explore the potential of the lattice strain model, as derived from studies of mineral-melt partitioning, to be used as a geothermometer. By testing our approach to estimating temperature with both eclogitic and peridotitic minerals we have demonstrated the versatility of the lattice strain model as a thermometer for mantle minerals. Through focusing on garnet and cpx, which are stable over a very wide range of temperature and pressure conditions, we have developed a model that has very wide-reaching applications, both in metamorphic geology, tectonic reconstructions and diamond exploration. Whilst the focus of this paper is on the partitioning of garnet

565 and cpx the approach taken here can be applied to any coexisting mineral pair, as
566 long as a method exists to calculated E and r for the minerals of interest. In light of
567 recent predictive models for plagioclase-melt partitioning of trace elements
568 (Dohmen and Blundy 2014) the potential of cpx-plagioclase pairs as trace element
569 geothermometers would benefit from further evaluation. It also stands to reason
570 that this approach could be used to estimate T from mineral-melt partitioning data,
571 which can be applied to volcanic systems.

572

573

574

575 **Acknowledgements**

576 JP is grateful to Rio Tinto for a PhD studentship at the University of Bristol, B.G.I. and
577 Dave Dobson for access to their multi-anvil apparatus and Richard Hinton for
578 assistance with the ion-microprobe analyses. JB acknowledges funding from ERC
579 Advanced Grant CRITMAG and a Royal Society Wolfson Research Merit Award. This
580 work has benefitted from discussion with Chris Smith, Russell Sweeney, John
581 Schumacher, Susanne Skora and Wim van Westrenen. We thank Yan Liang and an
582 anonymous reviewer for thoughtful reviews of our manuscript.

583
584 **References**

585 Adam, J., and Green, T. (2006) Trace element partitioning between mica- and
586 amphibole-bearing garnet lherzolite and hydrous basanitic melt: 1.
587 Experimental results and the investigation of controls on partitioning
588 behaviour. Contributions to Mineralogy and Petrology, 152, 1–17.

589 Ai, Y. (1994) A revision of the garnet-clinopyroxene Fe2+-Mg exchange
590 geothermometer. Contributions to Mineralogy and Petrology, 115, 467–
591 473.

592 Allan, N.L., Du, Z., Lavrentiev, M.Y., Blundy, J.D., Purton, J.A., and Westrenen, W.
593 van (2003) Atomistic simulation of mineral–melt trace-element
594 partitioning. Physics of the Earth and Planetary Interiors, 139, 93 – 111.

595 Appleyard, C.M., Bell, D.R., and le Roex, A.P. (2007) Petrology and geochemistry
596 of eclogite xenoliths from the Rietfontein kimberlite, Northern Cape.
597 Contributions to Mineralogy and Petrology, 154, 309–333.

598 Bennett, S., Blundy, J., and Elliott, T. (2004) The effect of sodium and titanium on
599 crystal-melt partitioning of trace elements. Geochimica et Cosmochimica
600 Acta, 68, 2335–2347.

601 Berry, A.J., Yaxley, G.M., Woodland, A.B., and Foran, G.J. (2010) A XANES
602 calibration for determining the oxidation state of iron in mantle garnet.
603 Chemical Geology, 278, 31–37.

604 Blundy, J., and Wood, B. (1994) Prediction of crystal-melt partition coefficients
605 from elastic-moduli. Nature, 372, 452–454.

606 Brice, J. (1975) Some thermodynamic aspects of growth of strained crystals.
607 Journal of Crystal Growth, 28, 249–253.

608 Deer, W.A., Howie, R.A., and Zussman, J. (1992) An introduction to the Rock
609 Forming Minerals Vol. 2. Prentice Hall.

610 Dohmen, R., and Blundy, J.D. (2014) A predictive thermodynamic model for
611 element partitioning between plagio- clase and melt as a function of
612 pressure, temperature and composition. American Journal Of Science,
613 314, 1310–1372.

614 Ellis, D., and Green, D. (1979) An experimental study of the effect of Ca upon
615 garnet-clinopyroxene Fe-Mg exchange equilibria. Contributions to
616 Mineralogy and Petrology, 71, 13–22.

617 Frost, B.R., and Chacko, T. (1989) The granulite uncertainty principle -
618 Limitations on thermobarometry in granulites. Journal of Geology, 97,
619 435–450.

620 Goldschmidt, V. (1937) The principles of distribution of chemical elements in
621 minerals and rocks. The seventh Hugo Muller Lecture, delivered before
622 the Chemical Society on March 17th, 1937. Journal Of The Chemical
623 Society, 655–673.

624 Gréau, Y., Huang, J.-X., Griffin, W.L., Renac, C., Alard, O., and O'Reilly, S.Y. (2011)
625 Type I eclogites from Roberts Victor kimberlites: Products of extensive
626 mantle metasomatism. Geochimica et Cosmochimica Acta, 75, 6927–6954.

627 Green, T., Blundy, J., Adam, J., and Yaxley, G. (2000) SIMS determination of trace
628 element partition coefficients between garnet, clinopyroxene and hydrous
629 basaltic liquids at 2-7.5 GPa and 1080-1200 oC. Lithos, 53, 165–187.

630 Griffin, W.L., and Ryan, C.G. (1995) Trace elements in indicator minerals: area
631 selection and target evaluation in diamond exploration. Journal of
632 Geochemical Exploration, 53, 311.

633 Hanger, B.J., Yaxley, G.M., Berry, A.J., and Kamenetsky, V.S. (2015) Relationships
634 between oxygen fugacity and metasomatism in the Kaapvaal subcratonic
635 mantle, represented by garnet peridotite xenoliths in the Wesselton
636 kimberlite, South Africa. Lithos, 212, 443–452.

637 Hanrahan, M., Brey, G., Woodland, A., Altherr, R., and Seitz, H. (2009) Towards a
638 Li barometer for bimineralic eclogites: experiments in CMAS.
639 Contributions to Mineralogy and Petrology, Online.

640 Harte, B., and Kirkley, M.B. (1997) Partitioning of trace elements between
641 clinopyroxene and garnet: Data from mantle eclogites. Chemical Geology,
642 136, 1–24.

643 Hauri, E., Wagner, T., and Grove, T. (1994) Experimental and natural partitioning
644 of Th, U, Pb and other trace elements between garnet, clinopyroxene and
645 basaltic melts. Chemical Geology, 117, 149–166.

646 Hinton, R. (1990) Ion microprobe trace-element analysis of silicates-
647 Measurement of multi-element glasses. Chemical Geology, 83, 11–25.

648 Irving, A.J., and Frey, F.A. (1978) Distribution of trace-elements between garnet
649 megacrysts and host volcanic liquids of kimberllitic to rhyolitic
650 composition. Geochimica et Cosmochimica Acta, 42, 771–787.

651 Klein, M., Stosch, H., Seck, H., and Shimizu, N. (2000) Experimental Partitioning of
652 High Field Strength and Rare Earth Elements Between Clinopyroxene and
653 Garnet in Andesitic to Tonalitic Systems. Geochimica et Cosmochimica
654 Acta, 64, 99–115.

655 Klemme, S., Blundy, J., and Wood, B. (2002) Experimental constraints on major
656 and trace element partitioning during partial melting of eclogite.
657 Geochimica et Cosmochimica Acta, 66, 3109–3123.

658 Klimm, K., Blundy, J.D., and Green, T.H. (2008) Trace element partitioning and
659 accessory phase saturation during H2O-saturated melting of basalt with
660 implications for subduction zone chemical fluxes. Journal of Petrology, 49,
661 523–553.

662 Kuzyura, A.V., Wall, F., Jeffries, T., and Litvin, Y.A. (2010) Partitioning of trace
663 elements between garnet, clinopyroxene and diamond-forming
664 carbonate-silicate melt at 7 GPa. Mineralogical Magazine, 74, 227–239.

665 Lee, C.-T.A., Harbert, A., and Leeman, W.P. (2007) Extension of lattice strain
666 theory to mineral/mineral rare-earth element partitioning: An approach
667 for assessing disequilibrium and developing internally consistent
668 partition coefficients between olivine, orthopyroxene, clinopyroxene and
669 basaltic melt. Geochimica et Cosmochimica Acta, 71, 481–496.

670 Li, Y., Zheng, Y., and Fu, B. (2005) Mossbauer spectroscopy of omphacite and
671 garnet pairs from elogites: Application to geothermobarometry. American
672 Mineralogist, 90, 90–100.

673 Matjuschkin, V., Brey, G.P., Hoefer, H.E., and Woodland, A.B. (2014) The influence
674 of Fe3+ on garnet-orthopyroxene and garnet-olivine geothermometers.
675 Contributions to Mineralogy and Petrology, 167.

676 McDade, P., Wood, B., and Blundy, J. (2002a) Experimental determination of
677 near-solidus peridotite trace partition coefficients. Geochimica et
678 Cosmochimica Acta, 66, A499.

679 McDade, P., Wood, B., Van Westrenen, W., Brooker, R., Gudmundsson, G., Soulard,
680 H., Najorka, J., and Blundy, J. (2002b) Pressure corrections for a selection
681 of piston-cylinder cell assemblies. Mineralogical Magazine, 66, 1021–
682 1028.

683 Morimoto, N., Fabries, J., Ferguson, A.K., Ginzburg, I.V., Ross, M., Seifert, F.A., and
684 Zussman, J. (1988) Nomenclature of pyroxenes. American Mineralogist,
685 73, 1123–1133.

686 Nagasawa, H. (1966) Trace Element Partition Coefficient In Ionic Crystals.
687 Science, 152, 767–&.

688 Nakamura, D. (2009) A new formulation of garnet-clinopyroxene
689 geothermometer based on accumulation and statistical analysis of a large
690 experimental data set. Journal of Metamorphic Geology, 27, 495–508.

691 Pattison, D.R.M. (1994) Are Reversed Fe-Mg Exchange And Solid-Solution
692 Experiments Really Reversed. American Mineralogist, 79, 938–950.

693 Powell, R. (1985) Regression diagnostics and robust regression in
694 geothermometer geobarometer calibration - The garnet clinopyroxene
695 geothermometer revisited. Journal of Metamorphic Geology, 3, 231–243.

Raheim, A., and Green, D. (1974) Experimental determination of temperature and pressure-dependence of Fe-Mg partition coefficient for coexisting garnet and clinopyroxene. Contributions to Mineralogy and Petrology, 48, 179–203.

Rubatto, D., and Hermann, J. (2007) Experimental zircon/melt and zircon/garnet trace element partitioning and implications for the geochronology of crustal rocks. Chemical Geology, 241, 38–61.

Ryerson, F.J., and Hess, P.C. (1978) Implications of liquid-liquid distribution coefficients to mineral-liquid partitioning. Experimental trace element geochemistry, 42, 921–932.

Salters, V.J.M., and Longhi, J. (1999) Trace Element Partitioning During the Initial Stages of Melting Beneath Mid-Ocean Ridges. Earth and Planetary Science Letters, 166, 15–30.

Salters, V.J.M., Longhi, J., and Bizimis, M. (2002) Near Mantle Solidus Trace Element Partitioning at Pressures up to 3.4 GPa. Geochemistry Geophysics Geosystems, 3.

Schmidt, M., Connolly, J., Gunther, D., and Bogaerts, M. (2006) Element partitioning: The role of melt structure and composition. Science, 312, 1646–1650.

Schumacher, J.C. (1991) Empirical ferric iron corrections - Necessity, assumptions and effects on selected geothermobarometers. Mineralogical Magazine, 55, 3–18.

Shannon, R. (1976) Revised Effective Ionic-Radii And Systematic Studies Of Interatomic Distances In Halides And Chalcogenides. Acta Crystallographica Section A, 32, 751–767.

Simakov, S.K. (2008) Garnet-clinopyroxene and clinopyroxene geothermobarometry of deep mantle and crust eclogites and peridotites. Lithos, 106, 125–136.

Sun, C., and Liang, Y. (2012) Distribution of REE between clinopyroxene and basaltic melt along a mantle adiabat: effects of major element composition, water, and temperature. Contributions to Mineralogy and Petrology, 163, 807–823.

——— (2013) The importance of crystal chemistry on REE partitioning between mantle minerals (garnet, clinopyroxene, orthopyroxene, and olivine) and basaltic melts. Chemical Geology, 358, 23 – 36.

——— (2015) A REE-in garnet-clinopyroxene thermobarometer for eclogites, granulites and garnet peridotites. Chemical Geology, 393-394, 79–92.

Tuff, J., and Gibson, S.A. (2007) Trace-element partitioning between garnet, clinopyroxene and Fe-rich picritic melts at 3 to 7 GPa. Contributions to Mineralogy and Petrology, 153, 369–387.

Van Orman, J.A., Grove, T.L., Shimizu, N., and Layne, G.D. (2002) Rare earth element diffusion in a natural pyrope single crystal at 2.8 GPa. Contributions to Mineralogy and Petrology, 142, 146.

Van Westrenen, W. (2000) Thermodynamics of garnet-melt partitioning. University of Bristol.

Van Westrenen, W., and Draper, D.S. (2007) Quantifying garnet-melt trace element partitioning using lattice-strain theory: new crystal-chemical and thermodynamic constraints. Contributions to Mineralogy and Petrology, 154, 717–730.

Van Westrenen, W., Blundy, J., and Wood, B. (1999) Crystal-chemical controls on trace element partitioning between garnet and anhydrous silicate melt. American Mineralogist, 84, 838–847.

Van Westrenen, W., Blundy, J., and Wood, B. (2000) Effect of Fe2+ on garnet-melt trace element partitioning: experiments in FCMAS and quantification of crystal-chemical controls in natural systems. Lithos, 53, 189–201.

Watson, E.B. (1976) Two-Liquid Partition Coefficients: Experimental Data and Geochemical Implications. Contributions to Mineralogy and Petrology, 56, 119–134.

Withers, A.. (1997) Water in the Mantle. University of Bristol.

Witt-Eickschen, G., and O'Neill, H. (2005) The effect of temperature on the equilibrium distribution of trace elements between clinopyroxene, orthopyroxene, olivine and spinel in upper mantle peridotite. Chemical Geology, 221, 65–101.

Wood, B.J., and Blundy, J.D. (1997) A predictive model for rare earth element partitioning between clinopyroxene and anhydrous silicate melt. Contributions to Mineralogy and Petrology, 129, 166–181.

——— (2001) The effect of cation charge on crystal-melt paritioning of trace elements. Earth and Planetary Science Letters, 188.

Yao, L., and Liang, Y. (2015) Closure temperature in cooling bi-mineralic systems: I. Definition and with application to REE-in-two-pyroxene thermometer. Geochimica et Cosmochimica Acta, 162, 137–150.

Figures

Figure 1. Schematic representation of the terms in the lattice strain model taken from Wood and Blundy (1997). The Nernst partition coefficient describes the partitioning of an element between a mineral and melt. The parameters are defined in the text.

Figure 2. SEM images of typical experimental run products demonstrating homogenous grains, indicative of equilibrium. **a** is a piston cylinder experiment, RD25, at 1200 °C and 3.4 GPa. **b** is a multi-anvil experiment, V545, at 1400 °C and 10 GPa. The scale bar is 100 μm in both cases.

Figure 3. Spider diagram of partition coefficients between garnet and cpx for trace element data generated in this research. **a** is JP1 starting composition, **b** is BAS and c is the AOB, ZrTi and NSR-16 starting mixes.

Figure 4. Experimental REE partitioning between garnet and cpx as a function of ionic radius of the element. The red line shows the weighted fit calculated using **Equation 2** with values of *D* and *r* calculated by the method of Wood and Blundy (1997) and van Westrenen and Draper (2007). Error bars show 1 s.d. of the mean.

Figure 5. Experimental REE partitioning between garnet and cpx as a function of ionic radius of the element. The red line shows the weighted fit calculated using **Equation 2** with values of *D* and *r* calculated by the method of Wood and Blundy (1997) and van Westrenen and Draper (2007). Error bars show 1 s.d. of the mean.

Figure 6. Comparison of values of E^{grt} calculated through the model of Sun and Liang (2013) ($E_{(S\&L)}$) with those found with the model van Westrenen and Draper (2007) ($E_{(vW\&D)}$) using the experimental the garnet-cpx data set.

Figure 7. The effect of change in *T* on the partitioning of REE. The black lines use the same experimental data values for E and r and change only *T* from 800 to 1400 °C in 200 °C intervals.

Figure 8. a. Comparison of experimental temperature with *T* found through a weighted mean of REE pairs, from Nd to Lu, and the lattice strain model, **Equation 3**. Error bars are shown where larger than symbol. The red circles are experiments from this study and the black diamonds are those from the literature, see **Table 5**. The mean absolute deviation is only 75 °C for all the data. b. Comparison of calculated *T* using the weighted mean temperature using all

REE pairs lattice strain model ($T_{(JP)}$) with the *T* found using Ellis and Green (1979) ($T_{(EG)}$) and Sun and Liang (2015) ($T_{(SL)}$), which have a mean absolute deviation of 240 and 278 ^{o}C respectively. In both figures the black line shows the 1:1 relationship.

Figure 9: Comparison of isothermal, isochemical experiments to show the effect of pressure. The temperature is the experimental *T*.

Figure S1: Graphs showing published data with red fit line calculated using the methods of Wood and Blundy (1997) and van Westrenen and Draper (2007). The superscript 1 denotes data are normalized to Yb, superscript 2 are normalized to Eu and superscript 3 denotes Er, as opposed to Y, as no Y partitioning data are available.

Figure S2: See **Figure S1** for explanation.

Figure S3: See **Figure S1** for explanation.

This is a preprint, the final version is subject to change, of the American Mineralogist (MSA)
Cite as Authors (Year) Title. American Mineralogist, in press.
(DOI will not work until issue is live.) DOI: http://dx.doi.org/10.2138/am-2016-5427

Table 1: Cpx wt% EMPA data

Experiment	BL58		RD25		G21		V547		V546		V545		BL88		RD56		G25		RD56 AOB		UCL3		RB627	
Starting Comp.	JP 1		JP 1		JP 1		JP 1		JP 1		JP 1		BAS		BAS		BAS		AOB		ZrTi		NSR-16	
T	1200		1200		1200		1400		1400		1400		1100		1200		1200		1200		1120		970	
P	3.0		3.4		6.0		6.0		8.0		10.0		3.0		3.0		5.0		3.0		5.0		1.3	
t	6		4		7		6		6		6		48		48		7		48		10		123	
n	20		11		6		20		29		14		21		3		3		17		8		6	
SiO_2	53.07	(32)	54.75	(24)	56.00	(76)	54.21	(78)	56.17	(37)	56.55	(30)	51.12	(66)	50.27	(56)	52.65	(42)	51.01	(38)	53.80	(36)	48.4	(41)
TiO_2	0.07	(2)	0.05	(1)	0.39	(57)	0.06	(2)	0.17	(1)	0.14	(1)	0.88	(22)	0.70	(4)	0.35	(3)	0.44	(2)	0.46	(10)	1.21	(15)
Al_2O_3	4.29	(40)	3.49	(40)	9.44	(107)	9.18	(85)	9.39	(78)	8.84	(51)	6.78	(67)	7.65	(34)	6.07	(62)	5.61	(24)	5.23	(31)	8.14	(47)
Cr_2O_3	1.11	(40)	0.94	(41)	0.44	(28)	0.02	(2)	0.68	(15)	0.68	(8)	0.07	(4)	0.08	(2)	0.08	(2)	0.50	(14)	0.03	(1)		
FeO	3.77	(15)	4.06	(27)	3.17	(110)	4.07	(27)	4.60	(29)	4.77	(19)	6.06	(32)	6.66	(27)	4.81	(15)	6.97	(30)	5.45	(50)	11.88	(155)
MnO	0.10	(1)	0.12	(1)	0.05	(3)	0.06	(2)	0.04	(1)	0.04	(1)	0.11	(2)	0.09	(1)	0.07	(1)	0.11	(1)	0.13	(1)	0.29	(6)
MgO	17.79	(42)	19.77	(76)	11.17	(132)	12.60	(45)	10.69	(46)	10.24	(27)	12.87	(59)	12.54	(20)	13.66	(50)	14.01	(30)	15.03	(27)	10.91	(89)
CaO	17.87	(49)	15.54	(136)	14.39	(134)	13.91	(50)	13.00	(67)	12.54	(42)	19.28	(24)	18.48	(26)	18.32	(22)	18.83	(33)	16.97	(35)	16.64	(110)
Na_2O	1.54	(11)	1.62	(12)	5.67	(47)	4.70	(36)	5.52	(34)	6.43	(25)	2.19	(19)	2.64	(10)	3.25	(31)	1.95	(14)	2.04	(10)	1.5	(41)
K_2O	b.d.		b.d.		b.d.		0.66	(11)	0.23	(2)	0.35	(2)	b.d.		0.01	(4)	b.d.		b.d.		b.d.		0.01	(1)
ZrO_2																					0.02	(2)		
Total	99.62		100.33		100.71		99.49		100.49		100.58		99.36		99.13		99.27		99.44		99.13		98.98	
c.p.f.u.																								
Si	1.91		1.95		1.97		1.93		1.99		2.00		1.87		1.84		1.91		1.87		1.96		1.82	
$Al^{(iv)}$	0.09		0.05		0.03		0.07		0.01		0.00		0.13		0.16		0.09		0.13		0.04		0.18	
$Al^{(vi)}$	0.10		0.09		0.37		0.32		0.39		0.37		0.17		0.17		0.16		0.11		0.19		0.19	
Ti	0.00		0.00		0.01		0.00		0.00		0.00		0.02		0.02		0.01		0.01		0.01		0.03	
Cr	0.03		0.03		0.01		0.00		0.02		0.02		0.00		0.00		0.00		0.01		0.00		0.00	
Fe^{3+}	0.06		0.04		0.02		0.10		0.00		0.07		0.06		0.13		0.14		0.12		0.00		0.03	
Fe^{2+}	0.05		0.08		0.08		0.02		0.14		0.07		0.12		0.07		0.01		0.10		0.17		0.34	
Mn	0.00		0.00		0.00		0.00		0.00		0.00		0.00		0.00		0.00		0.00		0.00		0.01	
Mg	0.96		1.05		0.59		0.67		0.57		0.54		0.70		0.69		0.74		0.77		0.82		0.61	
Ca	0.69		0.59		0.54		0.53		0.49		0.47		0.76		0.73		0.71		0.74		0.66		0.67	
Na	0.11		0.11		0.39		0.32		0.38		0.44		0.16		0.19		0.23		0.14		0.14		0.11	
K	0.00		0.00		0.00		0.03		0.01		0.02		0.00		0.00		0.00		0.00		0.00		0.00	
Zr																					0.00			

This is a preprint, the final version is subject to change, of the American Mineralogist (MSA)
Cite as Authors (Year) Title. American Mineralogist, in press.
(DOI will not work until issue is live.) DOI: http://dx.doi.org/10.2138/am-2016-5427

Starting comp. refers to table S1, *T* is in °C, P is in GPa, *t* is in hours, *n* is the number of analyses, b.d. is below detection and the parentheses show one standard deviation, e.g. 53.07 (11) should read 53.07 ±0.11, c.p.f.u. stands for cations per formula unit and are calculated based on 4 cations. The Fe^{3+} is calculated using the method of Schumacher (1991).

Table 2: Garnet wt% EMPA data

Experiment	BL58		RD25		G21		V547		V546		V545		BL88		RD56		G25		RD56 AOB		UCL3		RB627	
Starting Comp.	JP 1		JP 1		JP 1		JP 1		JP 1		JP 1		BAS		BAS		BAS		AOB		ZrTi		NSR-16	
T	1200		1200		1200		1400		1400		1400		1100		1200		1200		1200		1120		970	
P	3.0		3.4		6.0		6.0		8.0		10.0		3.0		3.0		5.0		3.0		5.0		1.3	
n	30		4		12		25		13		13		12		20		12		20		21		4	
SiO_2	41.82	(28)	41.48	(38)	42.60	(50)	42.39	(46)	42.74	(29)	43.45	(33)	39.56	(51)	40.58	(38)	39.56	(51)	40.24	(38)	41.04	(45)	38.61	(34)
TiO_2	0.16	(12)	0.27	(2)	0.24	(21)	0.11	(2)	0.36	(4)	0.44	(4)	0.78	(18)	0.61	(12)	0.78	(18)	0.51	(5)	1.46	(54)	0.94	(37)
Al_2O_3	21.38	(53)	20.71	(96)	22.60	(58)	21.91	(47)	21.30	(28)	20.23	(36)	21.98	(40)	21.86	(39)	21.98	(40)	21.11	(28)	21.03	(65)	21.29	(20)
Cr_2O_3	2.24	(83)	4.35	(105)	1.21	(77)	1.23	(41)	1.02	(27)	0.89	(15)	0.19	(4)	0.26	(11)	0.19	(4)	0.92	(20)	0.91	(71)		
FeO	6.56	(79)	7.81	(15)	8.03	(35)	6.63	(29)	7.71	(28)	7.45	(12)	12.26	(32)	12.65	(14)	12.26	(32)	13.15	(15)	7.97	(159)	19.4	(66)
MnO	0.26	(2)	0.25	(2)	0.24	(3)	0.22	(1)	0.22	(1)	0.23	(4)	0.34	(2)	0.40	(2)	0.34	(2)	0.40	(2)	0.29	(3)	1.07	(14)
MgO	21.05	(75)	19.28	(31)	18.79	(48)	20.10	(40)	18.52	(51)	17.76	(36)	13.69	(58)	14.94	(20)	13.69	(58)	15.49	(24)	20.00	(189)	11.77	(31)
CaO	6.51	(54)	6.96	(50)	7.31	(57)	7.43	(18)	8.67	(72)	9.86	(44)	10.91	(64)	9.05	(34)	10.91	(64)	8.16	(28)	6.34	(132)	6.45	(60)
Na_2O	0.03	(2)	0.03	(1)	0.14	(9)	0.18	(14)	0.30	(3)	0.56	(4)	0.15	(2)	0.11	(2)	0.15	(2)	0.04	(5)	0.12	(3)	0.06	(7)
K_2O	b.d.		b.d.		b.d.		0.01	(1)	0.01	(1)	0.01	(1)	0.01	(3)	b.d.		0.01	(3)	b.d.		b.d.		b.d.	
ZrO_2																					0.17	(6)		
Total	100.01		101.14		101.16		100.21		100.86		100.88		99.88		100.45		99.88		100.02		99.33		99.59	
c.p.f.u.																								
Si	2.96		2.95		3.00		2.99		3.02		3.08		2.90		2.95		2.90		2.94		2.95		2.91	
Al	1.78		1.74		1.88		1.82		1.78		1.69		1.90		1.87		1.90		1.82		1.78		1.89	
Ti	0.01		0.01		0.01		0.01		0.02		0.02		0.04		0.03		0.04		0.03		0.08		0.05	
Cr	0.13		0.24		0.07		0.07		0.06		0.05		0.01		0.01		0.01		0.05		0.05		0.00	
Fe^{3+}	0.16		0.10		0.04		0.13		0.12		0.14		0.23		0.17		0.23		0.2		0.13		0.19	
Fe^{2+}	0.23		0.37		0.44		0.26		0.34		0.31		0.53		0.60		0.53		0.61		0.35		1.03	
Mn	0.02		0.02		0.01		0.01		0.01		0.01		0.02		0.02		0.02		0.02		0.02		0.07	
Mg	2.22		2.04		1.98		2.12		1.95		1.88		1.50		1.62		1.50		1.69		2.14		1.32	
Ca	0.49		0.53		0.55		0.56		0.66		0.75		0.86		0.70		0.86		0.64		0.49		0.52	
Na	0.00		0.00		0.02		0.03		0.04		0.08		0.02		0.02		0.02		0.01		0.02		0.01	
K	0.00		0.00		0.00		0.00		0.00		0.00		0.00		0.00		0.00		0.00		0.00		0.00	

This is a preprint, the final version is subject to change, of the American Mineralogist (MSA)
Cite as Authors (Year) Title. American Mineralogist, in press.
(DOI will not work until issue is live.) DOI: http://dx.doi.org/10.2138/am-2016-5427

Zr	0.01	

Abbreviations are the same as table 1 and calculations are based on 8 cations.

Table 3: Cpx trace element data measured by SIMS

Sample	BL58		RD25		G21		V547		V546		V545		BL88		RD56		G25		RD56 AOB		UCL3		RB627	
n	4		4		2		4		4		2		4		3		1		3		5		1	
Li	10.8	(6)	24	(4)	30.2	(1)	17.8	(4)	33	(2)	35	(3)	28	(2)	25	(1)	15	(3)	44	(1)	417	(20)	24	(5)
B	0.99	(7)	1.3	(2)	3.2	(6)	1.1	(2)	9	(1)	15.6	(6)	1.8	(4)	0.1	(1)	1.8	(4)	1.7	(5)	28	(3)	5.4	(11)
Sc	14.2	(7)	16	(1)	6.7	(7)	6.8	(9)	6.3	(2)	5.0	(5)	21	(2)	21.54	(8)	12	(4)	74	(7)	131	(6)	232	(46)
Ti	336	(10)	380	(173)	382	(33)	267	(13)	835	(19)	790	(98)	5667	(801)	3582	(125)	1832	(366)	2881	(773)	2053	(291)	5422	(1084)
V	20.4	(5)	64	(14)	40.1	(5)	23	(1)	33	(2)	34.9	(1)	309	(17)	135	(10)	243	(49)	67	(4)	72	(7)	534	(107)
Co	54	(2)	54	(6)	27.6	(1)	39	(1)	37	(2)	33	(2)	49	(3)	49	(3)	31	(6)	231	(7)	5.1	(6)	na	
Ga	50	(9)	na		na		68	(2)	77	(12)	93	(12)	na		na		na		na		na		na	
Sr	9	(1)	7	(1)	19.0	(5)	15.7	(8)	77	(1)	96	(22)	169	(7)	163	(2)	142	(28)	70	(6)	76	(8)	14.3	(29)
Y	2.2	(9)	1.5	(2)	0.8	(1)	1.03	(7)	1.11	(8)	0.9	(2)	4.8	(9)	4.41	(1)	2.3	(5)	9	(3)	10	(3)	111	(22)
Zr	0.7	(1)	1.0	(5)	17	(22)	0.5	(1)	1.5	(2)	4.6	(17)	48	(7)	27	(1)	22	(4)	5	(2)	134	(30)	91	(18)
Nb	0.16	(6)	0.4	(2)	0.7	(5)	0.18	(6)	1.2	(5)	4	(5)	0.5	(2)	0.26	(4)	0.25	(5)	14	(15)	0.11	(3)	5.2	(10)
Ba	0.14	(7)	0.06	(6)	3.4	(1)	0.5	(4)	2.1	(14)	0.44	(6)	0.7	(3)	0.4	(3)	2	(4)	2	(1)	0.04	(4)	12.4	(25)
La	2.1	(4)	1.0	(3)	1.0	(3)	0.15	(5)	0.4	(2)	0.8	(8)	4.2	(5)	3.4	(1)	1.8	(4)	11	(3)	5	(1)	47.1	(94)
Ce	1.4	(1)	0.8	(2)	2.7	(9)	0.9	(2)	2.7	(2)	3.4	(8)	14	(1)	10.1	(4)	6	(1)	30	(6)	17	(6)	22.9	(46)
Pr	na		na		na		na		na		na		2.5	(3)	1.79	(8)	1.1	(2)	0.04	(4)	na		na	
Nd	1.9	(3)	1.1	(3)	3.15	(2)	1.0	(3)	2.6	(4)	3	(1)	15	(2)	10.6	(6)	6	(1)	39	(3)	27	(9)	53	(11)
Sm	2.2	(9)	0.03	(2)	1.2	(5)	1.1	(3)	3.1	(5)	2.1	(4)	4.0	(5)	2.8	(4)	1.5	(3)	12.7	(8)	11	(3)	79	(16)
Eu	6.7	(6)	3.7	(6)	2.9	(1)	2.7	(4)	5.9	(4)	4.2	(6)	1.3	(1)	0.78	(2)	0.7	(1)	27	(2)	26	(8)	90	(18)
Gd	7.7	(10)	3.6	(9)	2.4	(4)	3.1	(4)	3.9	(3)	4	(1)	3.9	(6)	1.9	(6)	2.0	(4)	29	(3)	27	(8)	115	(23)
Tb	b.d.		b.d.		b.d.		b.d.		b.d.		b.d.		0.48	(8)	0.33	(3)	0.23	(5)	b.d.		b.d.		na	
Dy	na		na		na		na		na		na		2.8	(3)	1.7	(3)	1.3	(3)	2.6	(4)	na		na	
Ho	na		na		na		na		na		na		0.28	(3)	0.21	(1)	0.17	(3)	0.08	(5)	na		na	
Er	4.2	(5)	2.9	(6)	2.3	(5)	2.1	(6)	1.8	(3)	0.77	(3)	b.d.		0.5	(2)	0.36	(7)	22	(7)	20	(5)	74	(15)
Yb	4.6	(4)	3.3	(8)	1.3	(1)	2.1	(6)	1.9	(6)	1.6	(3)	0.4	(2)	0.4	(2)	0.5	(1)	28	(15)	19	(4)	na	
Lu	67	(7)	5.6	(3)	1.8	(3)	3.3	(6)	3.1	(6)	3.1	(4)	0.12	(3)	0.03	(2)	0.02	(3)	43	(16)	24	(5)	23.4	(47)
Hf	0.9	(4)	1.0	(5)	1.5	(3)	0.6	(2)	1.7	(2)	1.6	(6)	2.1	(3)	0.8	(4)	0.9	(2)	6	(1)	0.5	(2)	45	(9)
Ta	0.14	(7)	0.7	(3)	1.0	(9)	0.2	(7)	0.7	(7)	2	(3)	0.35	(4)	b.d.		0.21	(4)	7.3	(7)	0.12	(4)	1.8	(4)
Pb	5	(1)	na		na		0.07	(4)	42	(16)	29.1	(6)	na		na		na		na		na		na	

This is a preprint, the final version is subject to change, of the American Mineralogist (MSA)
Cite as Authors (Year) Title. American Mineralogist, in press.
(DOI will not work until issue is live.) DOI: http://dx.doi.org/10.2138/am-2016-5427

Th	0.13	(3)	0.1	(1)	1	(1)	0.09	(4)	2.2	(16)	11	(1)	0.23	(3)	0.3	(3)	0.17	(3)	8	(5)	0.4	(2)	na	
U	0.09	(5)	0.1	(1)	0.2	(3)	0.07	(4)	0.4	(3)	0.4	(3)	0.21	(5)	b.d.		0.15	(3)	5	(4)	0.15	(7)	na	

All values are the mean of *n* in ppm, *n* is the number of analyses. Where the number of grains analyzed is one then the S.D. is 20% of the measured value.

Table 4: Garnet trace element data measured by SIMS

Sample	BL58		RD25		G21		V547		V546		V545		BL88		RD56		G25		RD56 AOB		UCL3		RB627	
n	3		5		2		4		3		3		5		1		4		4		5		1	
Li	0.41	(9)	1.17	(4)	3.9	(5)	1.9	(1)	6.6	(1)	11.3	(6)	5	(1)	2.9	(6)	2.1	(3)	5	(1)	81	(11)	2.3	(5)
B	0.28	(4)	0.22	(3)	2	(3)	0.3	(2)	1.1	(2)	4	(2)	0.8	(6)	b.d.		0.4	(5)	0.4	(1)	6	(8)	0.42	(8)
Sc	72	(3)	112	(11)	44	(6)	48	(4)	47	(7)	40	(1)	84	(12)	71	(14)	51	(2)	268	(9)	604	(18)	702	(140)
Ti	578	(154)	1621	(221)	746	(105)	480	(25)	1752	(50)	2119	(131)	3629	(615)	2951	(590)	2951	(278)	2990	(511)	6641	(1521)	3191	(638)
V	60	(2)	113	(3)	74	(5)	57	(1)	62	(2)	63	(1)	247	(9)	105	(221)	171	(20)	78	(4)	98	(10)	343	(69)
Co	97	(3)	101	(5)	88	(2)	95	(1)	128	(18)	104	(3)	75	(2)	97	(19)	76	(3)	408	(9)	10.8	(6)	na	
Ga	53	(5)	na		na		64	(4)	114	(6)	114	(2)	na		na		na		na		na		na	
Sr	0.4	(3)	0.32	(7)	1	(2)	0.39	(8)	2.0	(4)	3.5	(7)	1.5	(3)	1.1	(2)	2.0	(9)	3	(4)	1	(1)	0.31	(6)
Y	22	(1)	35	(3)	14	(3)	15.0	(6)	19.4	(3)	15.4	(4)	72	(10)	62	(12)	39	(1)	98	(7)	50	(8)	1078	(216)
Zr	5.2	(9)	10.4	(9)	5	(1)	3.1	(4)	11	(2)	13	(3)	92	(21)	90	(18)	61	(8)	14	(3)	1492	(410)	87	(17)
Nb	b.d.		1.0	(3)	b.d.		0.18	(5)	0.46	(3)	1.1	(9)	0.29	(9)	0.21	(4)	0.3	(2)	b.d.		0.46	(6)	1.1	(2)
Ba	b.d.		0.04	(2)	b.d.		0.1	(2)	1.1	(5)	0.6	(5)	0.5	(4)	0.06	(1)	0.7	(6)	0.3	(1)	0.1	(1)	0.83	(17)
La	0.2	(2)	0.09	(3)	1.6	(-)	0.020	(1)	0.10	(2)	0.3	(2)	0.19	(5)	0.15	(3)	0.2	(1)	0.3	(1)	0.3	(4)	1.0	(2)
Ce	0.04	(16)	0.19	(6)	2	(2)	0.11	(6)	0.9	(2)	2	(1)	1.0	(2)	0.8	(2)	0.7	(3)	1.69	(9)	1.1	(1)	0.6	(1)
Pr	na		na		na		na		na		na		0.4	(1)	0.3	(1)	0.29	(8)	0.02	(1)	na		na	
Nd	0.6	(3)	1.0	(3)	1.7	(3)	0.6	(1)	2.2	(3)	2.3	(2)	4.4	(6)	4	(1)	3.2	(7)	20	(10)	4	(1)	5.3	(11)
Sm	2.0	(17)	0.02 54	(2)	2.17 7	(1)	2.0	(4)	7.3	(2)	6	(1)	3.6	(4)	3.3	(7)	2.7	(5)	17	(4)	5	(1)	29	(6)
Eu	11	(3)	15	(3)	7	(1)	7.2	(4)	19.7	(6)	16	(2)	1.9	(4)	2.15	(4)	1.6	(1)	56	(11)	16	(4)	67	(13)
Gd	19	(5)	22	(3)	9.8	(9)	12.4	(7)	20	(7)	17	(4)	7	(1)	5	(1)	5.3	(4)	88	(12)	26	(6)	146	(29)
Tb	b.d.		0.02	(1)	b.d.		b.d.		b.d.		b.d.		1.8	(2)	1.6	(3)	1.0	(2)	b.d.		0.03	(2)	na	
Dy	na		na		na		na		na		na		13	(2)	10	(2)	8	(1)	1.3	(7)	na		na	
Ho	na		na		na		na		na		na		3.0	(4)	2.6	(5)	1.72	(8)	0.2	(2)	na		na	
Er	57	(2)	90	(9)	30	(7)	25	(21)	45	(3)	22	(3)	b.d.		8	(2)	4.9	(6)	252	(20)	128	(17)	1131	(226)
Yb	103.3	(9)	176	(23)	49	(9)	64	(4)	75	(3)	47	(5)	10	(1)	b.d.		5	(1)	445	(30)	269	(29)	na	
Lu	228	(10)	379	(59)	103	(21)	136	(9)	149	(11)	113.0	(3)	12	(3)	8	(2)	1.0	(1)	767	(56)	491	(41)	1131	(211)
Hf	1.8	(9)	4.4	(6)	1.72	(8)	1.9	(3)	6	(1)	7	(2)	4	(1)	2.2	(4)	2.1	(4)	11	(3)	2.1	(6)	18.2	(36)
Ta	0.6	(5)	3.7	(4)	4	(6)	0.11	(5)	0.3	(1)	0.9	(6)	2.6	(5)	0.6	(1)	0.5	(2)	0.5	(2)	0.3	(1)	0.7	(1)
Pb	5.08	(4)	na		na		5	(2)	18	(7)	5	(4)	na		na		na		na		na		na	

Th	0.2	(3)	0.07	(3)	4.16	(-)	0.05	(2)	1	(1)	6	(8)	0.9	(2)	b.d.		0.16	(7)	0.4	(1)	0.5	(8)	na
U	0.2	(2)	0.7	(3)	0.9	(10)	0.12	(7)	0.2	(1)	0.7	(3)	0.23	(5)	0.06	(1)	0.2	(1)	0.5	(2)	0.4	(4)	na

All values are the mean of *n* in ppm, *n* is the number of analyses. Where the number of grains analyzed is one then the S.D. is 20% of the measured value.

Table 5: Temperature calculations

Sample	$P_{(exp)}$	$T_{(exp)}$	$T_{(JP)}$	$\sigma\ T_{(JP)}$	$\Delta T_{(JP)}$	$T_{(EG)}$	$\Delta T_{(EG)}$	$T_{(EG*)}$	$\Delta T_{(EG*)}$	$T_{(SL)}$	$\Delta T_{(SL)}$
BL58	3	1200	1188	31	12	1220	20	966	234	813	387
RD25	3.4	1200	1141	30	59	1166	34	1051	149	1202	2
G21	6	1200	1377	29	177	1487	287	1427	227	1502	302
V547	6	1400	1362	38	38	1037	363	886	514	1381	19
V546	8	1400	1456	28	56	2646	1246	2165	765	1505	105
V545	10	1400	1538	47	138	2066	666	1716	316	1737	337
BL88	3	1100	1038	23	62	1345	245	1149	49	1297	197
RD56	3	1200	960	16	240	1005	195	914	286	1300	100
G25	5	1200	1231	31	31						
RD56 AOB	3	1200	1382	64	182	1076	124	958	242	1370	170
UCL3	5	1120	1237	34	117	2144	1024	1758	638	1194	74
RB627	1.3	970	971	16	1	1392	442	1275	325	946	24
Adam and Green (2006)	3.5	1180	1253	39	73	1166	14	1112	68	1129	51
Bennett et al. (2004)	3	1330	1413	73	83						
Green et al. (2000)	4	1100	1178	20	78	1081	19	929	171	1276	176
Green et al. (2000)	3	1160	1077	17	83	1047	113	905	255	1125	35
Green et al. (2000)	4	1200	1121	9	79	1246	46	1160	40	1109	91
Klemme et al. (2002)	3	1400	1334	49	66						
Kuzyura et al. (2010)	7	1265	1579	52	314	1461	196	1470	205	-162	1427
Kuzyura et al. (2010)	7	1265	1474	39	209	1633	368	1618	353	-255	1520
McDade (unpublished)	3	1495	1537	29	42	1583	88	1395	100	1908	413
Salters and Longhi (1999)	2.8	1537	1591	64	54	1563	1	1425	137	1927	390
Salters and Longhi (1999)	2.8	1530	1493	49	37	1486	44	1367	163	1668	138
Salters and Longhi (1999)	2.8	1525	1502	53	23	1613	63	1389	161	1713	188
Salters et al. (2002)	2.8	1650	1581	125	69	1444	206	1015	635	1804	154
Tuff and Gibson (2007)	3	1475	1405	24	70	1385	90	1414	61	1779	304
Tuff and Gibson (2007)	3	1425	1487	27	62	1458	33	1373	52	1643	218
Tuff and Gibson (2007)	7	1750	1780	34	30	1489	261	1611	139		

Withers (1997)	3	1470	1410	16	60	1416	54	1375	95	1607	137
mean					88		240		245		278

$T_{(exp)}$ is the experimental temperature, $T_{(JP)}$ is the weighted mean temperature found iteratively using Equation 3 with multiple REE pairs. The error, σT, is propagated from the standard deviation of the ion probe data. In each case ΔT is the mean absolute difference between the experimental T and the calculated T. $T_{(EG)}$ is the temperature calculated with the method of Ellis and Green (1979), $T_{(EG*)}$ is the method of Ellis and Green (1979) where Fe valence is not considered and $T_{(SL)}$ is the temperature calculated with the method of Sun and Liang (2015). Gaps in the table are a result of the models being unable to calculate a temperature or the necessary data not being available. The mean value shows the mean temperature deviation of all the experiments, including Kuzyura et al. (2010).

This is a preprint, the final version is subject to change, of the American Mineralogist (MSA)
Cite as Authors (Year) Title. American Mineralogist, in press.
(DOI will not work until issue is live.) DOI: http://dx.doi.org/10.2138/am-2016-5427

857 **Table S1:** Experimental starting compositions

	JP1	BAS	AOB	ZrTi	NSR-16
SiO_2	51.66	44.82	44.68	44.95	51.70
TiO_2	0.34	2.5	2.48	11.20	1.30
Al_2O_3	13.85	14.73	14.46	12.22	19.52
FeO		11.03			9.46
Fe_2O_3	6.34		15.41	6.80	
MnO	0.15	0.19	0.18	0.16	0.26
MgO	13.74	9.69	10.21	13.07	5.40
CaO	9.94	10.05	9.00	7.43	8.61
Na_2O	2.69	4.01	2.58	0.83	3.35
K_2O	0.66	1.85	0.77	0.03	0.24
Cr_2O_3	0.62		0.25	0.59	
P_2O_5		0.94			0.17
ZrO_2				3.69	
Total	99.99	99.81	100.02	100.97	100.01

JP1 is a synthetic oxide mix, BAS is a natural basanite glass, from Green et al. (2000), AOB is a synthetic alkali olivine basalt and NSR-16 a synthetic basaltic glass.

858
859
860
861
862
863
864
865
866
867
868
869
870
871
872
873
874
875
876
877
878
879
880
881
882
883
884

885
886
887
888

889 **Table S2:** Trace elements and amount added to starting compositions.

890

	JP1 ppm	BAS* ppm	AOB ppm	ZrTi ppm	NSR-16 ppm
Zn	250	-	250	250	-
Ni	250	-	250	250	-
Co	250	-	250	-	-
Cr	250	-	250	-	-
V	100	-	100	100	300
Sc	100	-	100	300	150
Ti	100	-	100	-	-
Y	50	33	50	50	300
La	50	54	150	150	200
Ce	200	110	300	300	50
Nd	100	42	200	200	50
Sm	50	8.7	50	50	60
Eu	100	2.6	100	100	80
Gd	100	-	100	100	100
Er	100	-	100	100	250
Yb	150	2.2	150	150	-
Lu	250	0.3	250	250	200
Nb	200	-	200	200	-
Ta	200	5	300	300	50
Zr	50	286	50	-	150
Hf	50	5.3	50	50	50
Th	200	-	300	300	-
U	200	-	200	200	-
Pb	200	-	200	200	-
Sr	400	1094	400	400	100
Ga	100	18	100	100	-
Li	100	200	300	500	10
Ba	-	-	-	-	400
B	-	-	-	-	10

* trace elements in BAS are those measured by Green et al. (2000) except Li which was added for this study.

891
892
893
894
895
896
897

This is a preprint, the final version is subject to change, of the American Mineralogist (MSA)
Cite as Authors (Year) Title. American Mineralogist, in press.
(DOI will not work until issue is live.) DOI: http://dx.doi.org/10.2138/am-2016-5427

898 **Table S3:** List of published experimental studies included in our thermometer
899 evaluation with *T, P* and starting composition of data

900

Author	*T* (°C)	*P* (GPa)	Bulk
Adam and Green (2006)	1180	3.5	lherzolite
Bennett et al. (2004)	1330	3	CMAS eclogite
Green et al. (2000)	1200	4	tholeiite
Green et al. (2000)	1100	3	basanite
Green et al. (2000)	1160	4	tholeiite
Hauri et al. (1994)	1430	2.5	high Al basalt
Klein et al. (2000)	1100	1.5	granulite xenolith
Klein et al. (2000)	1050	1.5	granulite xenolith
Klemme et al. (2002)	1400	3	eclogite
Kuzyura et al. (2010)	1265	7	silicocarbonatite
Kuzyura et al. (2010)	1265	7	silicocarbonatite
McDade (unpublished)	1495	3	Garnet-Peridotite
Salters and Longhi (1999)	1537	2.8	MORB
Salters and Longhi (1999)	1530	2.8	MORB
Salters and Longhi (1999)	1525	2.8	MORB
Salters et al. (2002)	1600	2.8	MORB
Tuff and Gibson (2007)	1475	3	ferropicrite
Tuff and Gibson (2007)	1425	3	ferropicrite
Tuff and Gibson (2007)	1750	7	ferropicrite
Withers (1997)	1470	3	basalt
Withers (1997)	1487	3	basalt

901
902
903
904
905
906
907
908
909
910

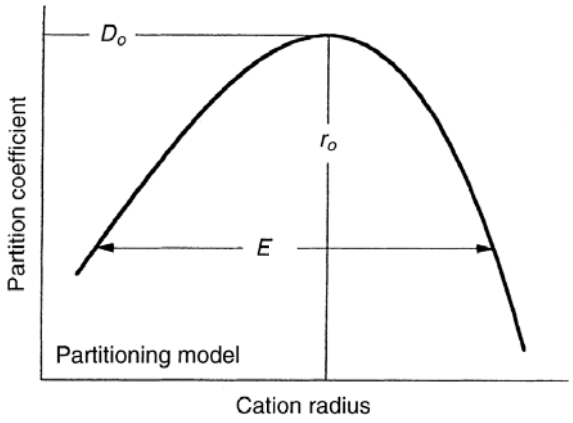

This is a preprint, the final version is subject to change, of the American Mineralogist (MSA)
Cite as Authors (Year) Title. American Mineralogist, in press.
(DOI will not work until issue is live.) DOI: http://dx.doi.org/10.2138/am-2016-5427

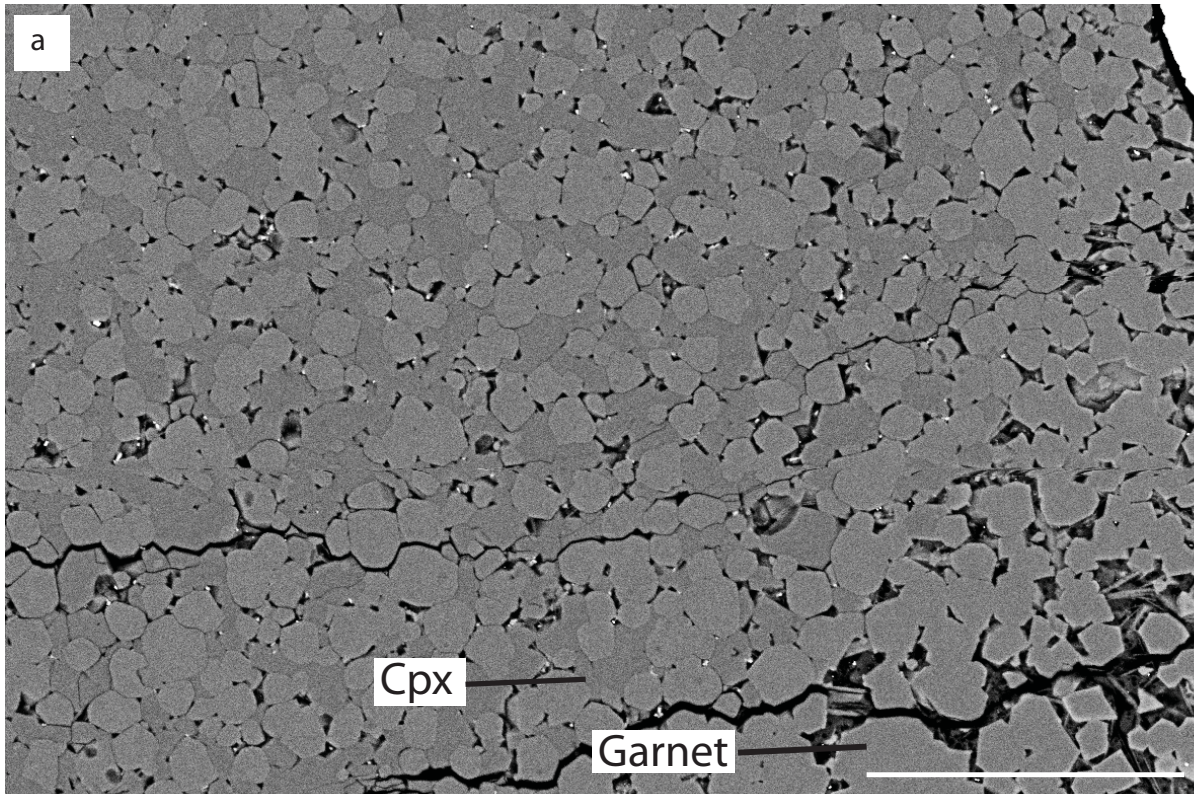

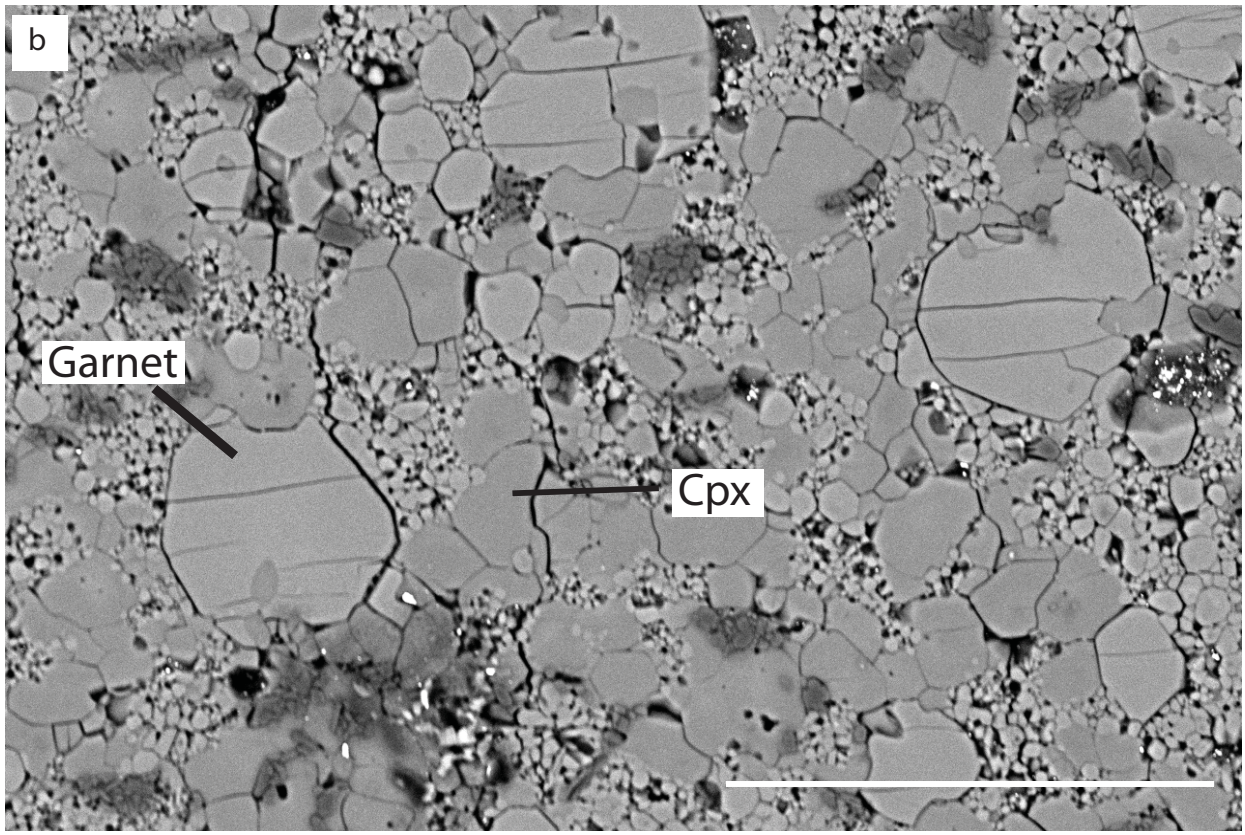

This is a preprint, the final version is subject to change, of the American Mineralogist (MSA)
Cite as Authors (Year) Title. American Mineralogist, in press.
(DOI will not work until issue is live.) DOI: http://dx.doi.org/10.2138/am-2016-5427

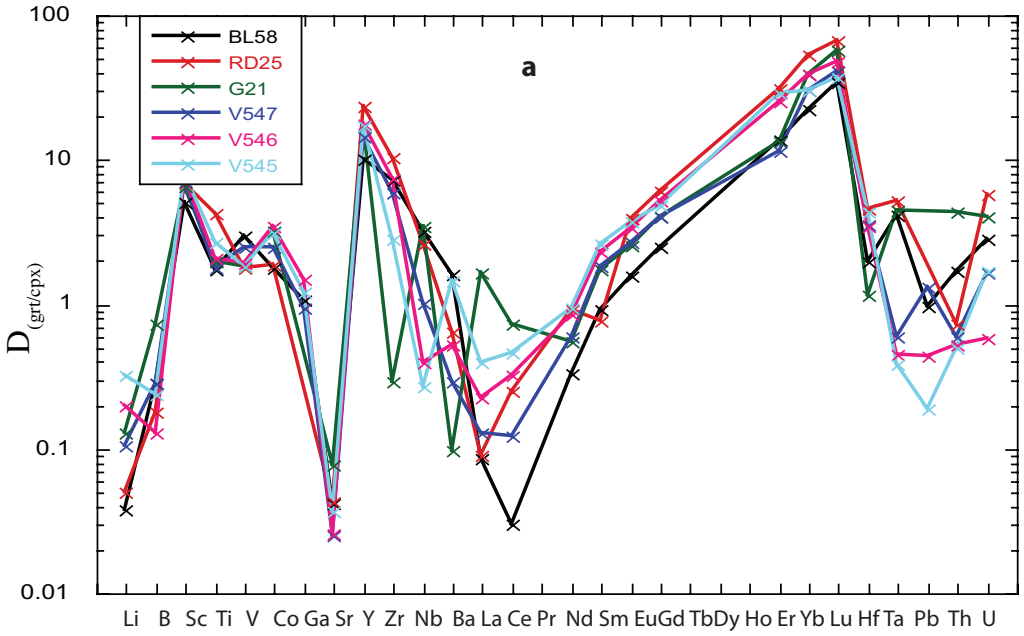

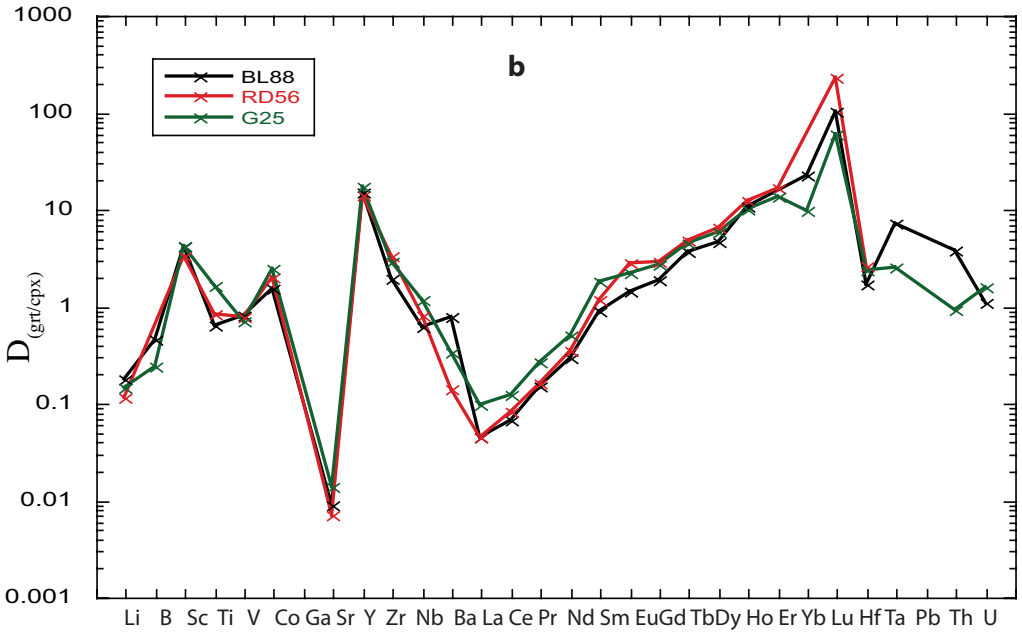

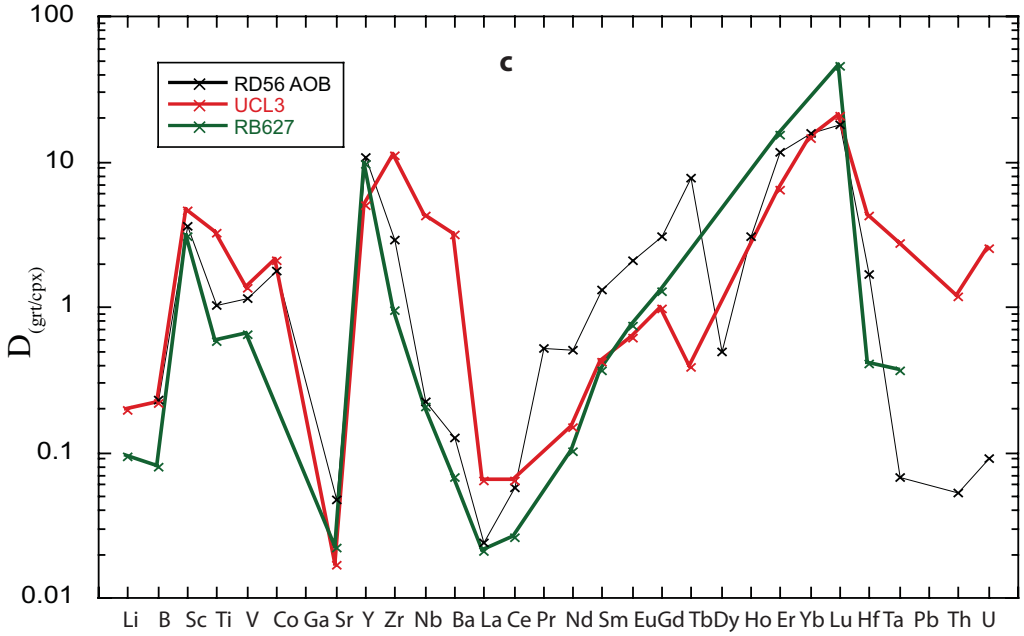

This is a preprint, the final version is subject to change, of the American Mineralogist (MSA)
Cite as Authors (Year) Title. American Mineralogist, in press.
(DOI will not work until issue is live.) DOI: http://dx.doi.org/10.2138/am-2016-5427

BL58

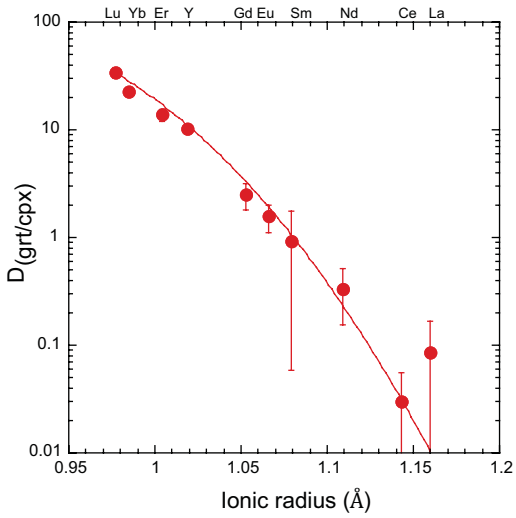

RD25

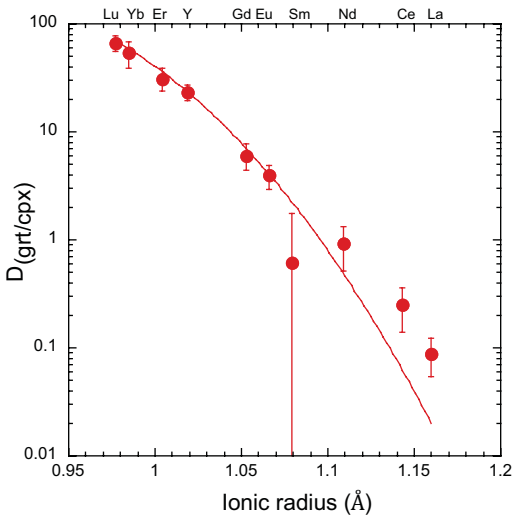

V547

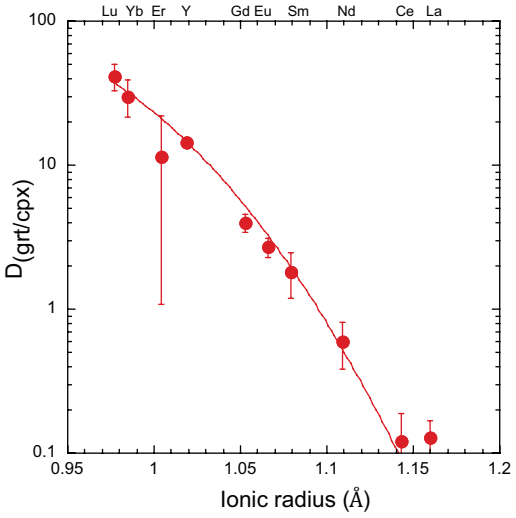

V546

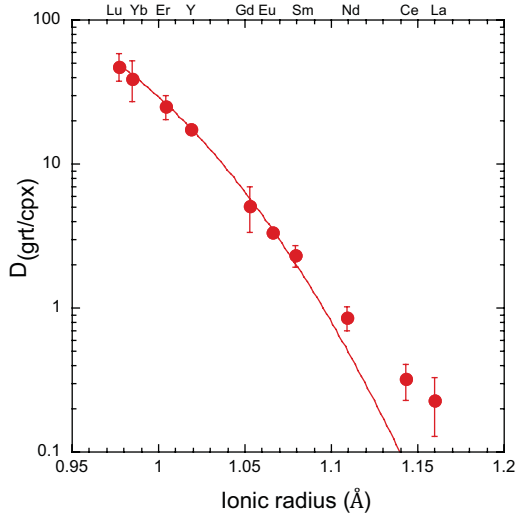

V545

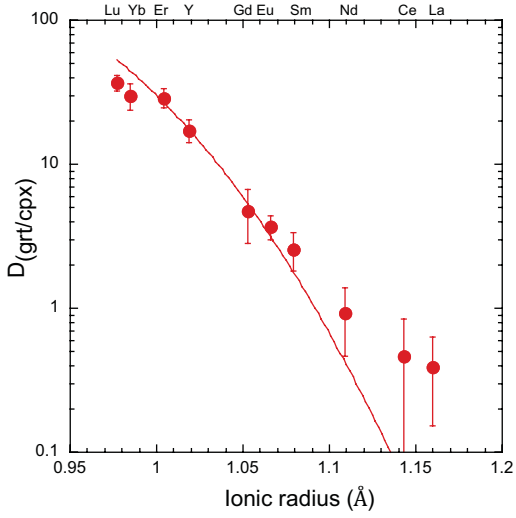

G21

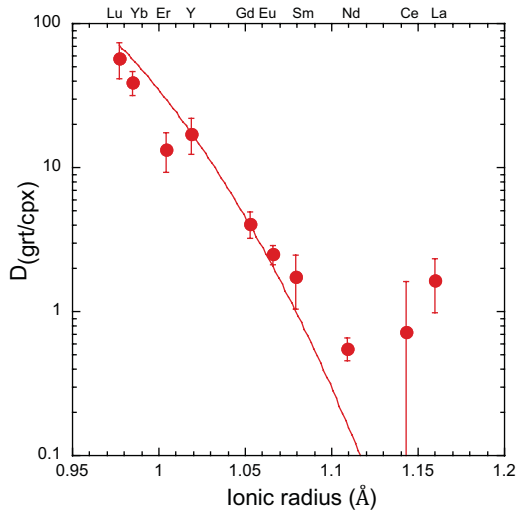

This is a preprint, the final version is subject to change, of the American Mineralogist (MSA)
Cite as Authors (Year) Title. American Mineralogist, in press.
(DOI will not work until issue is live.) DOI: http://dx.doi.org/10.2138/am-2016-5427

BL88

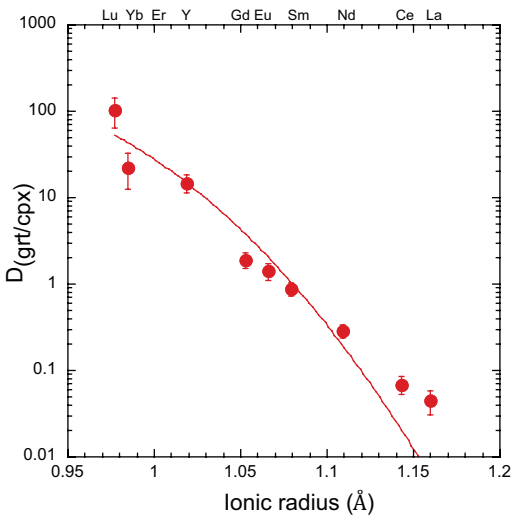

RD56

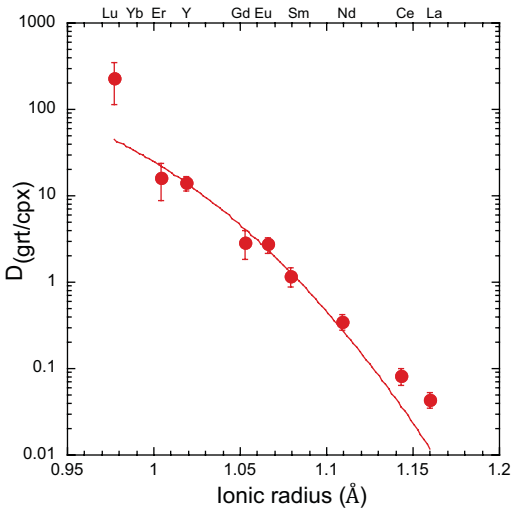

G25

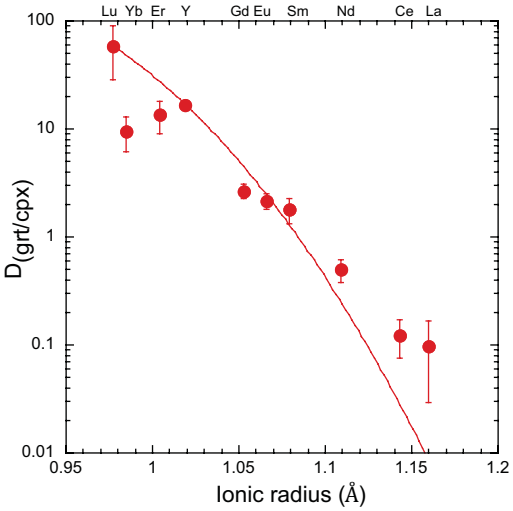

RD56 AOB

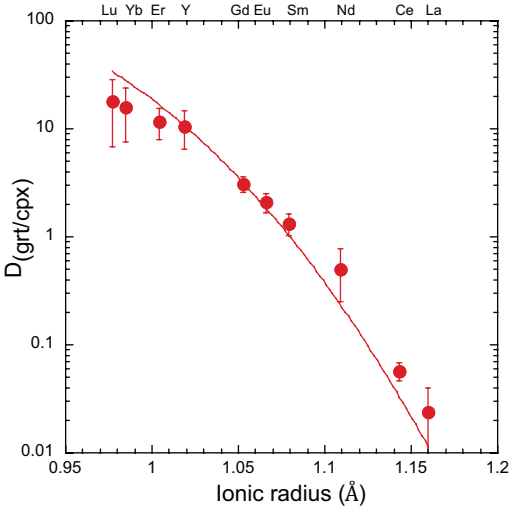

UCL3

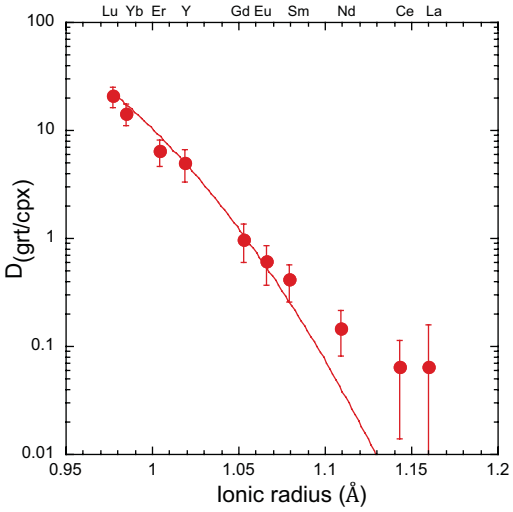

RB627

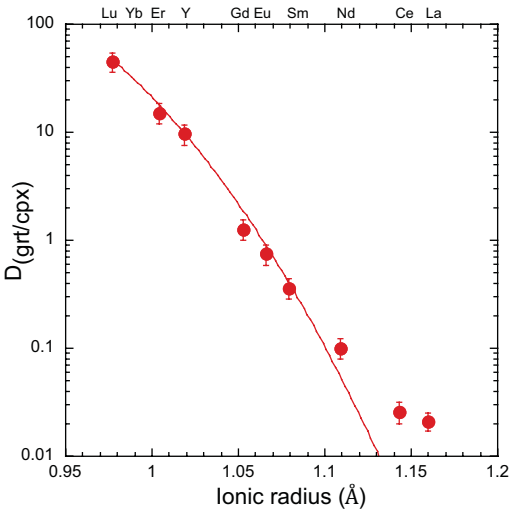

This is a preprint, the final version is subject to change, of the American Mineralogist (MSA)
Cite as Authors (Year) Title. American Mineralogist, in press.
(DOI will not work until issue is live.) DOI: http://dx.doi.org/10.2138/am-2016-5427

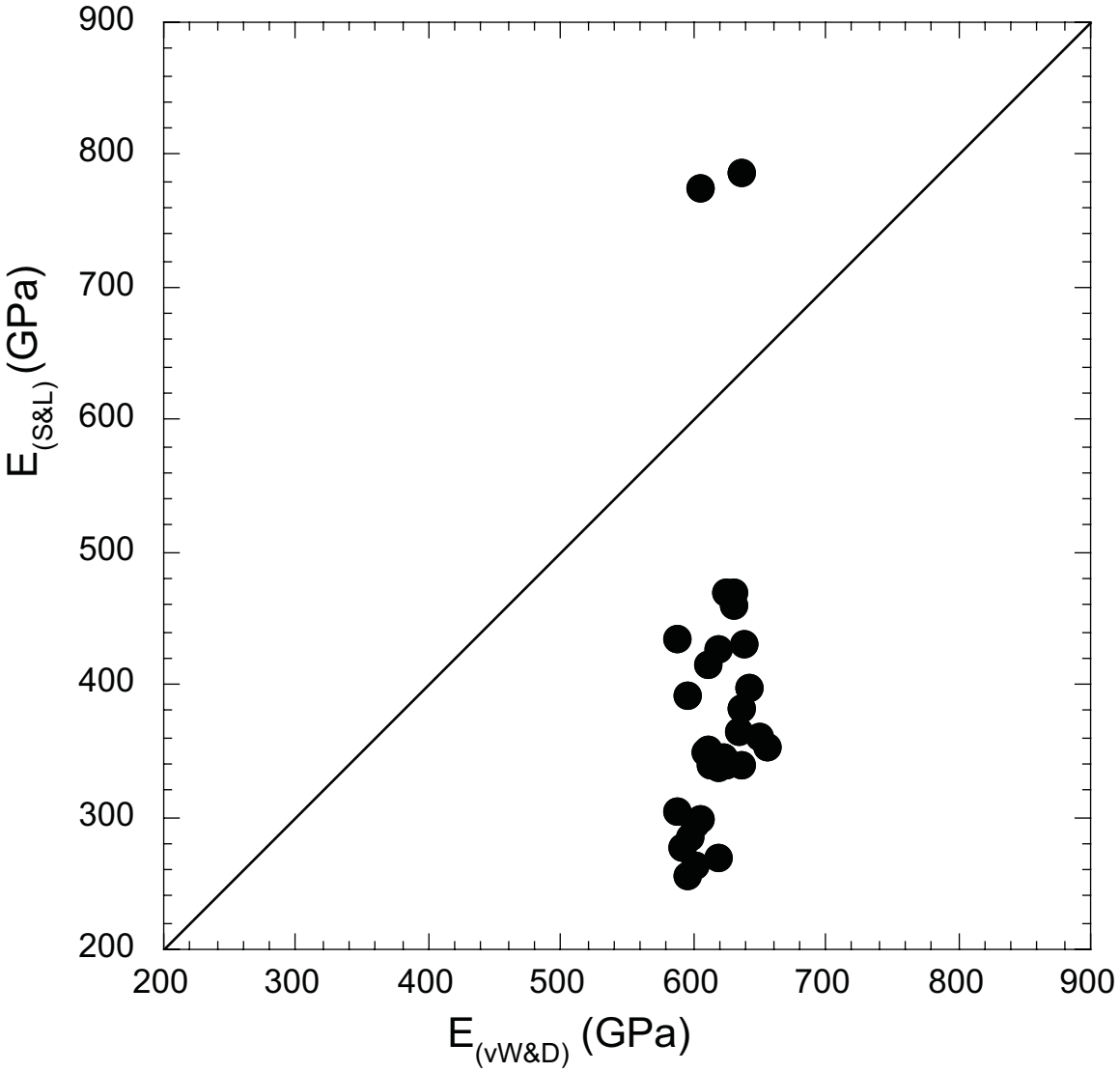

This is a preprint, the final version is subject to change, of the American Mineralogist (MSA)
Cite as Authors (Year) Title. American Mineralogist, in press.
(DOI will not work until issue is live.) DOI: http://dx.doi.org/10.2138/am-2016-5427

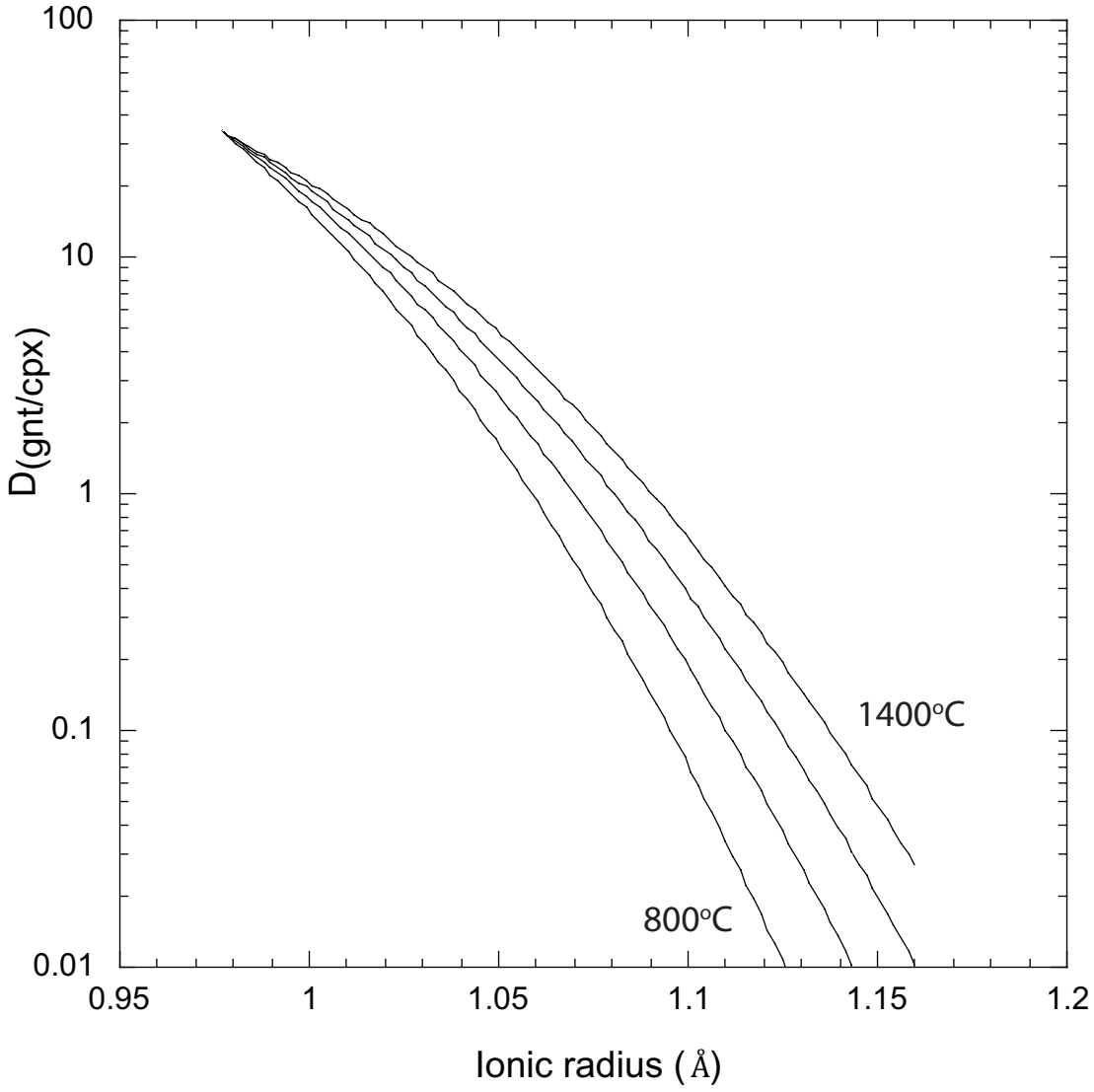

This is a preprint, the final version is subject to change, of the American Mineralogist (MSA)
Cite as Authors (Year) Title. American Mineralogist, in press.
(DOI will not work until issue is live.) DOI: http://dx.doi.org/10.2138/am-2016-5427

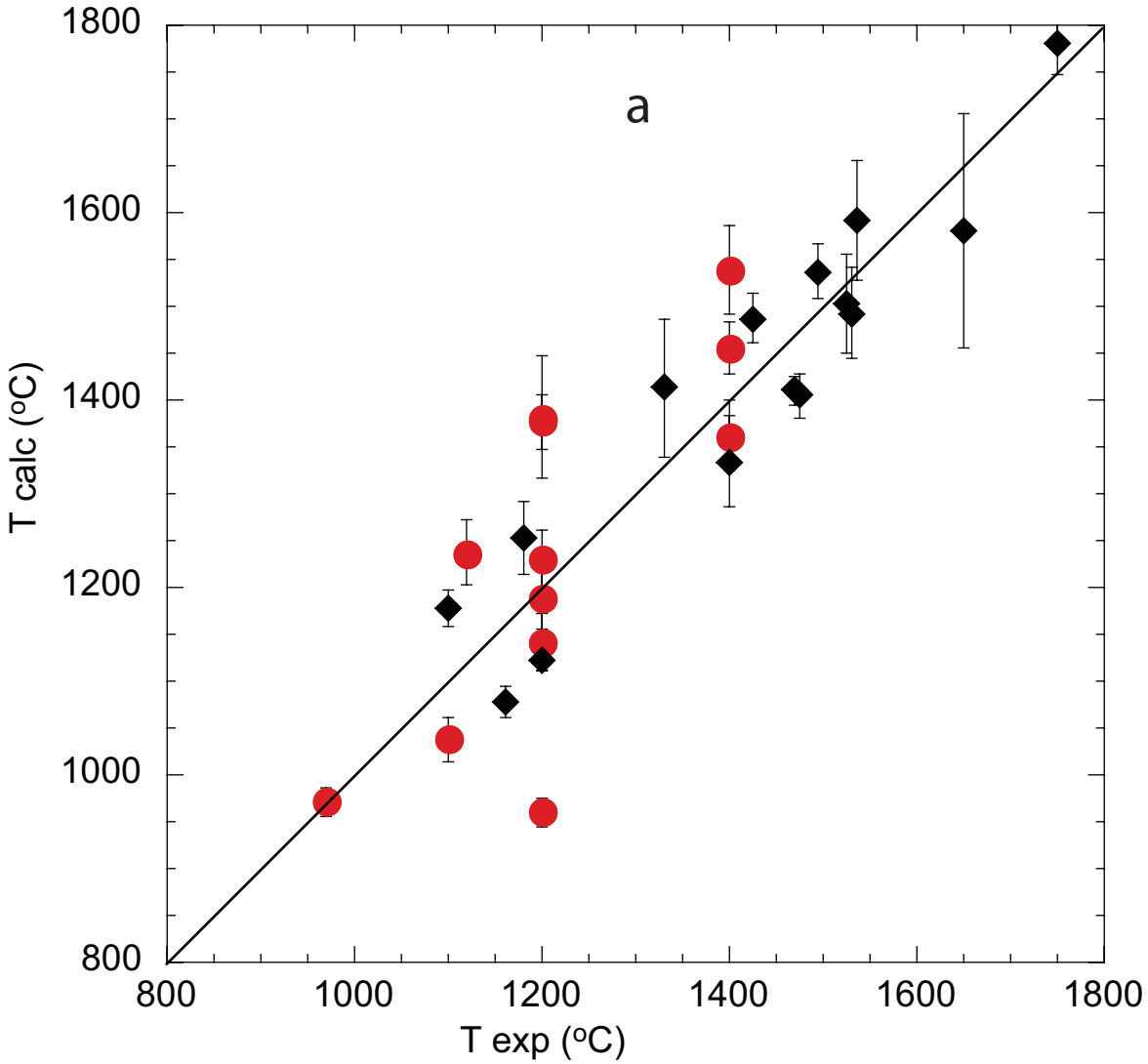

This is a preprint, the final version is subject to change, of the American Mineralogist (MSA)
Cite as Authors (Year) Title. American Mineralogist, in press.
(DOI will not work until issue is live.) DOI: http://dx.doi.org/10.2138/am-2016-5427

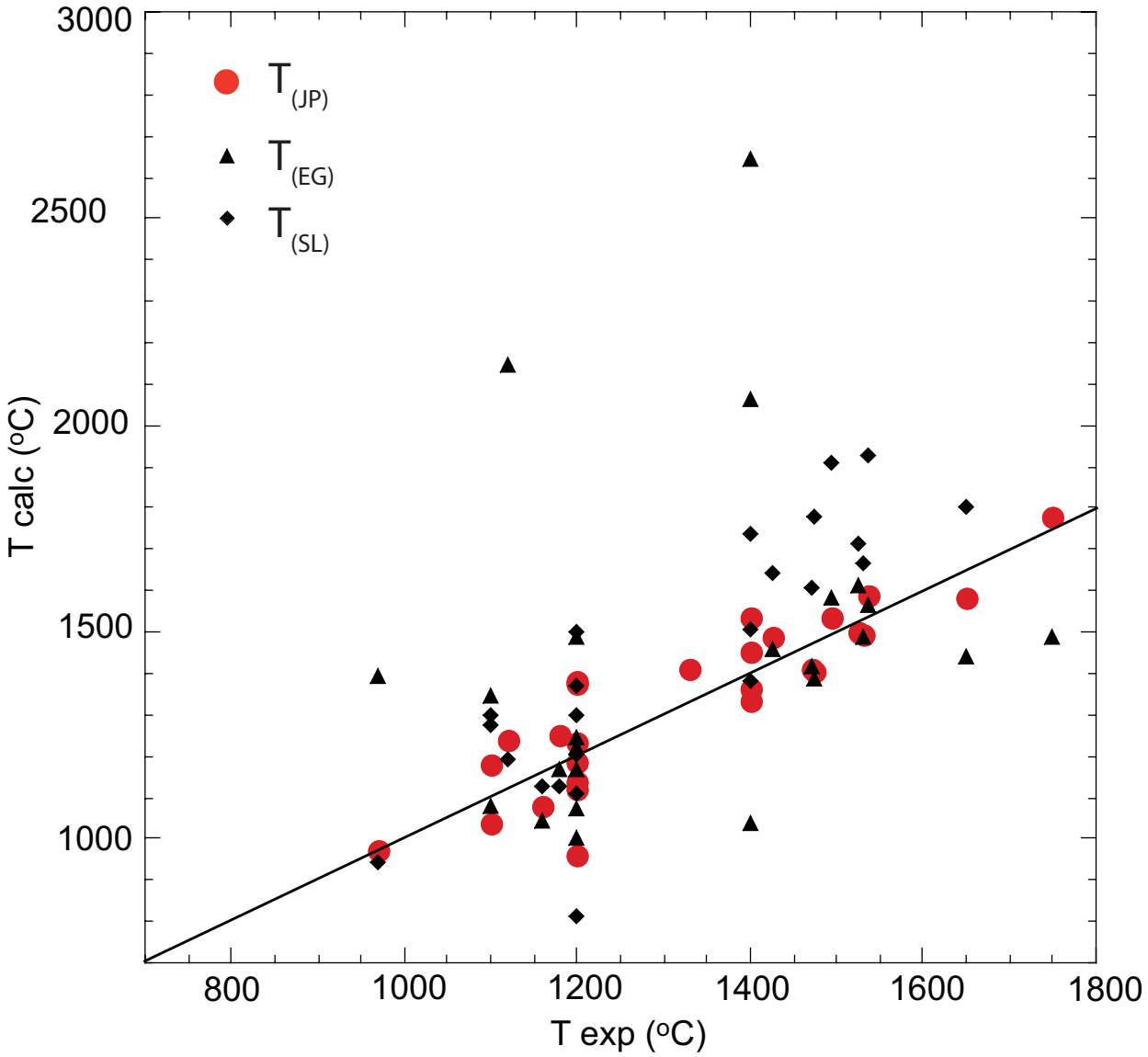

This is a preprint, the final version is subject to change, of the American Mineralogist (MSA)
Cite as Authors (Year) Title. American Mineralogist, in press.
(DOI will not work until issue is live.) DOI: http://dx.doi.org/10.2138/am-2016-5427

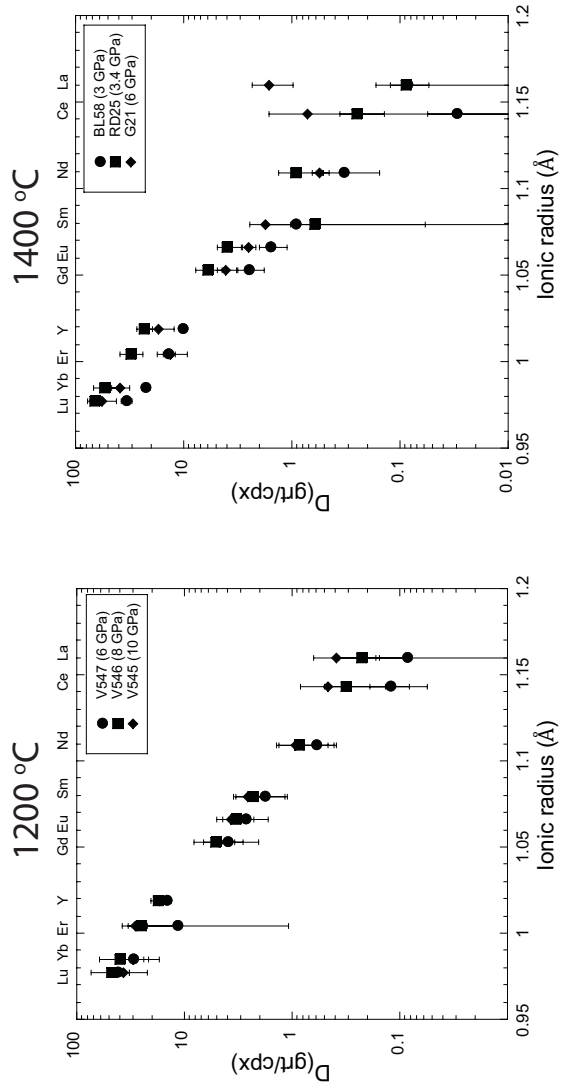

This is a preprint, the final version is subject to change, of the American Mineralogist (MSA)
Cite as Authors (Year) Title. American Mineralogist, in press.
(DOI will not work until issue is live.) DOI: http://dx.doi.org/10.2138/am-2016-5427

Adam and Green (2006)[1]

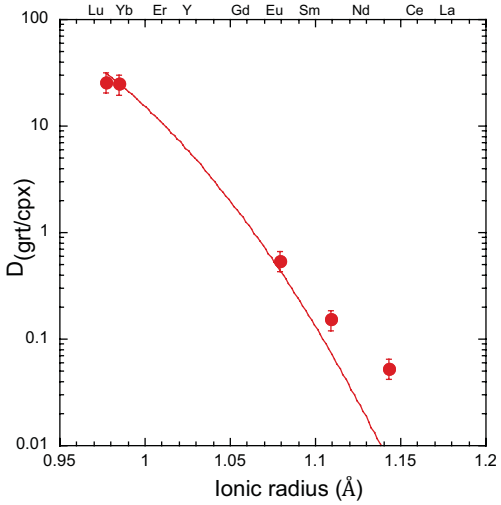

Bennett et al. (2004)

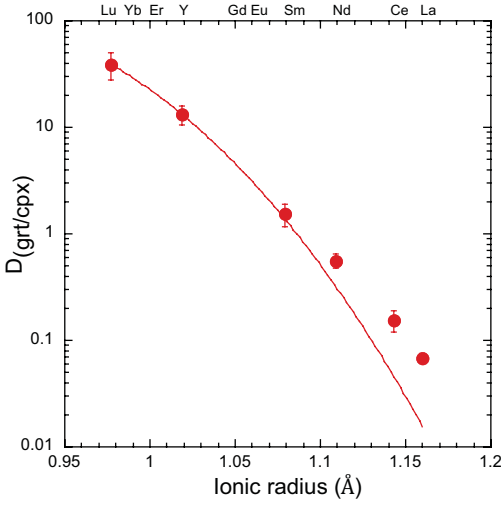

Green et al. (2000)
1787

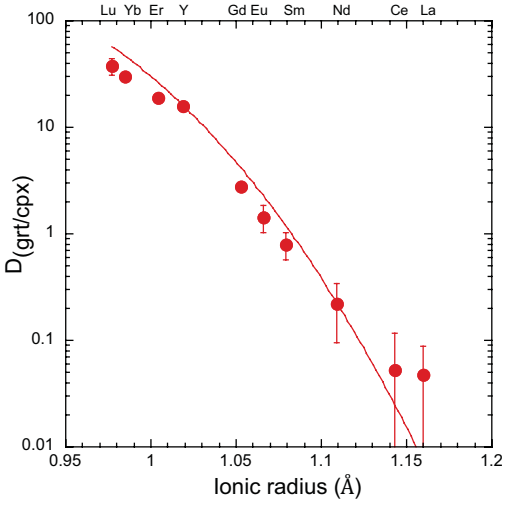

Green et al. (2000)
1798

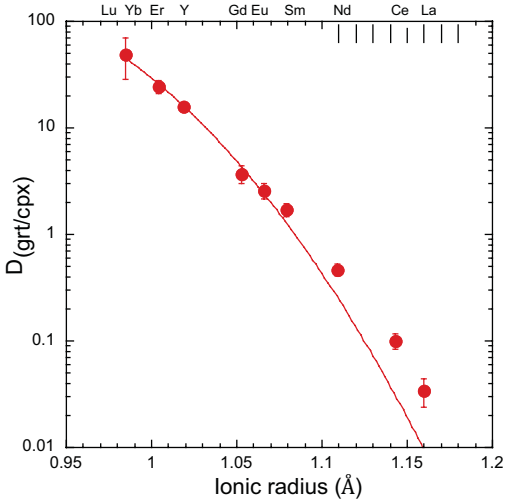

Green et al. (2000)
1807

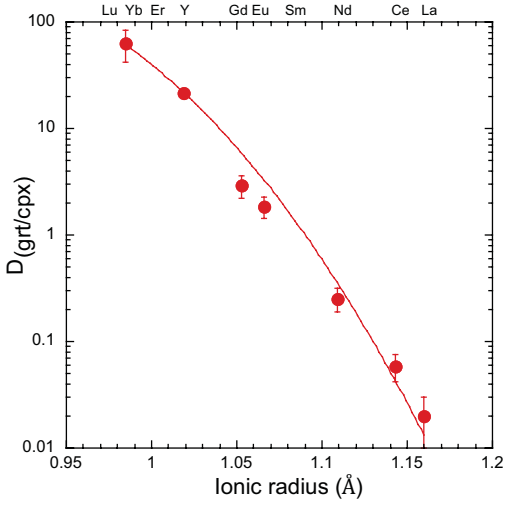

Hauri et al. (1994)[2]

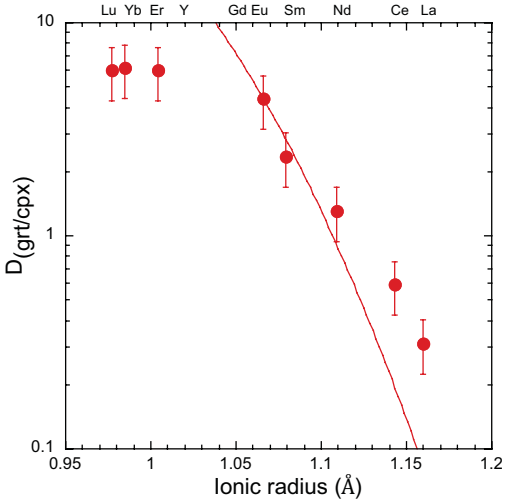

Klein et al. (2000)
1100

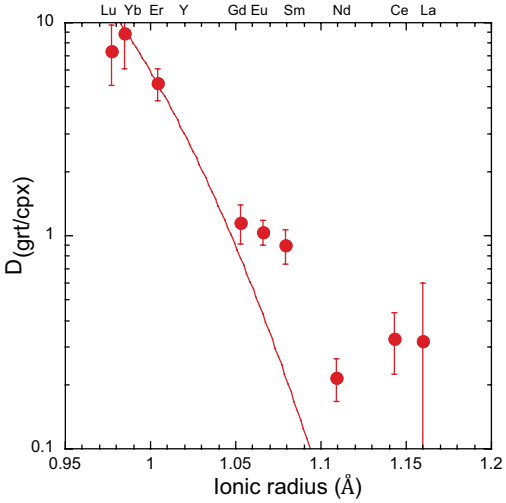

Klein et al. (2000)
1050

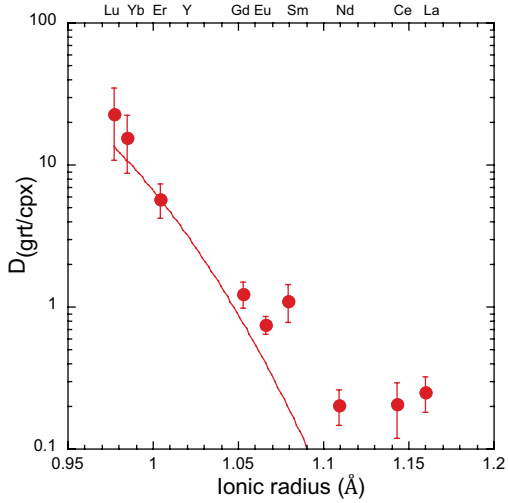

Klemme et al. (2002)

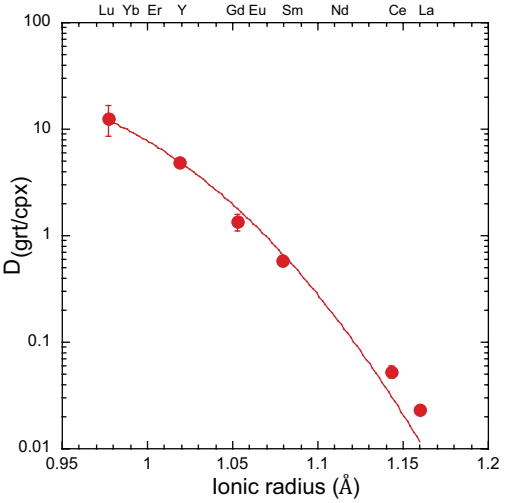

This is a preprint, the final version is subject to change, of the American Mineralogist (MSA)
Cite as Authors (Year) Title. American Mineralogist, in press.
(DOI will not work until issue is live.) DOI: http://dx.doi.org/10.2138/am-2016-5427

Kuzyura et al. (2010)[3]
2/1789a

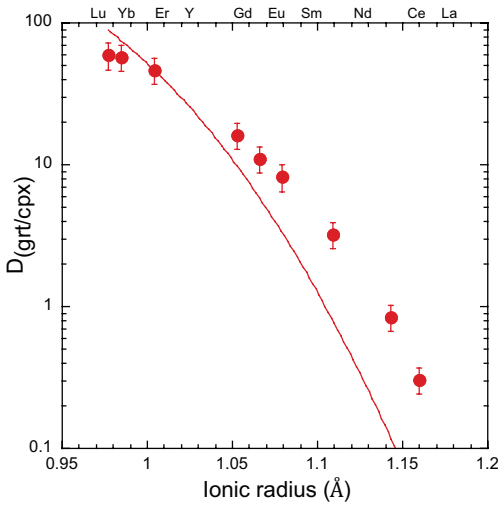

Kuzyura et al. (2010)[3]
2/17789b

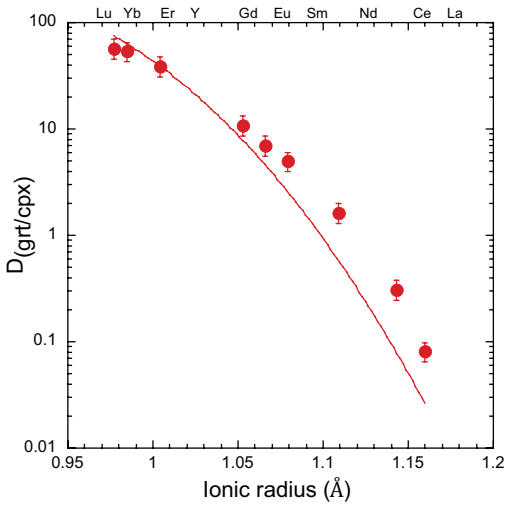

McDade

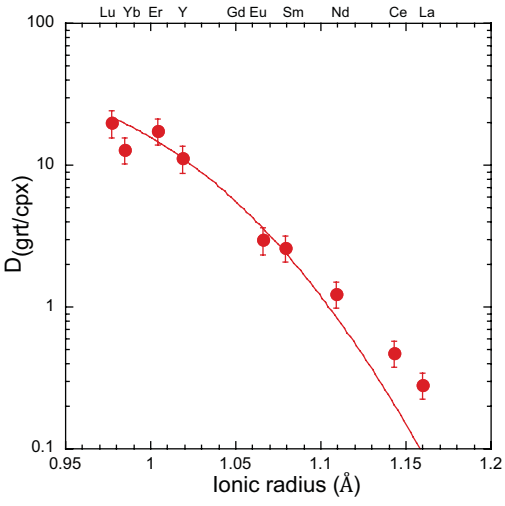

Salter and Longhi (1999)
TH694-6

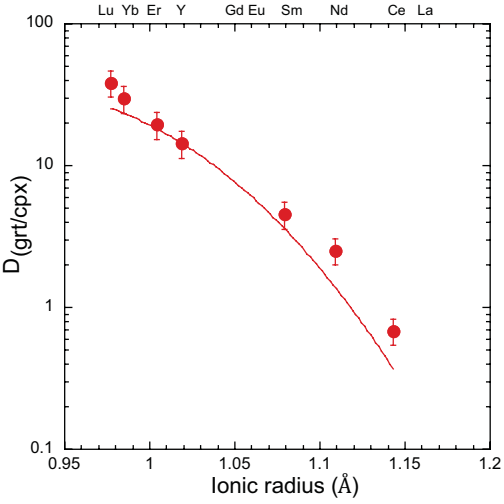

Salter and Longhi (1999)
M01295-3

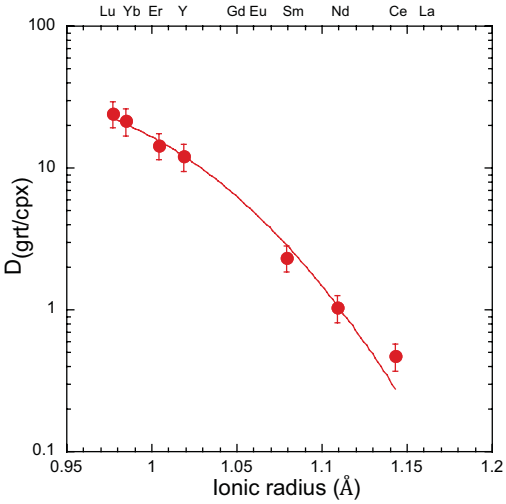

Salter and Longhi (1999)
TM694-3

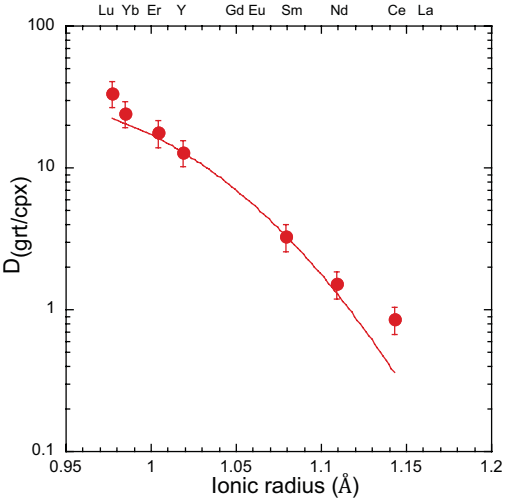

Salters et al. (2002)

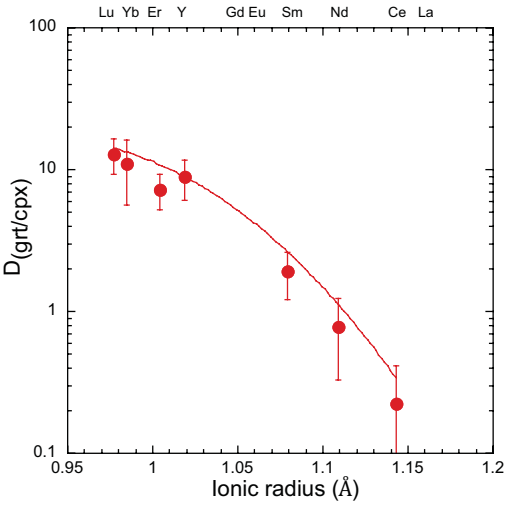

Tuff and Gibson (2007)
P511

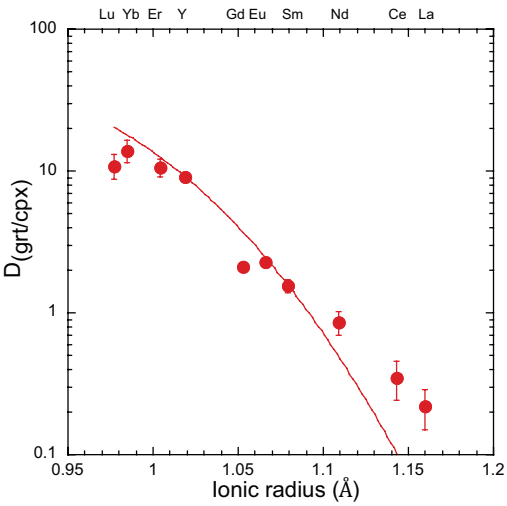

Tuff and Gibson (2007)
P529

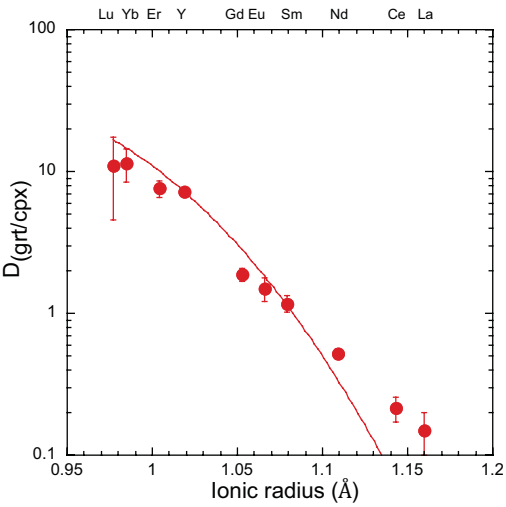

This is a preprint, the final version is subject to change, of the American Mineralogist (MSA)
Cite as Authors (Year) Title. American Mineralogist, in press.
(DOI will not work until issue is live.) DOI: http://dx.doi.org/10.2138/am-2016-5427

Tuff and Gibson (2007)
S1330

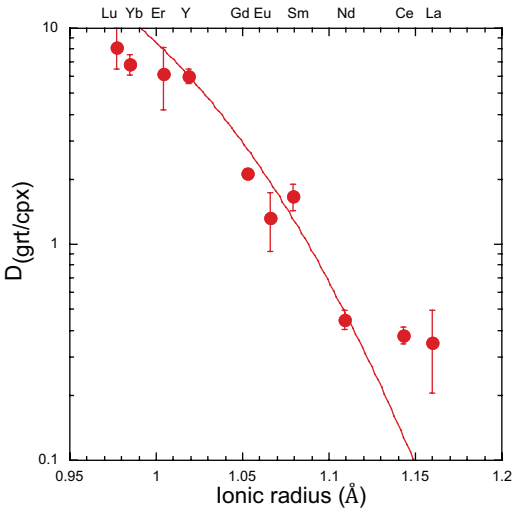

Withers (1997)

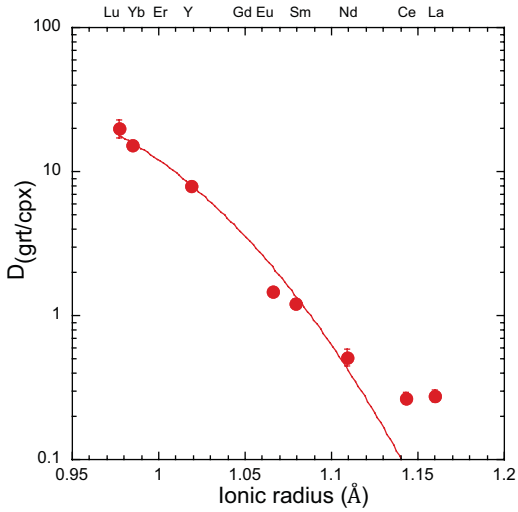

Withers (1997)